# Water soluble, multifunctional antibody-porphyrin gold nanoparticles for targeted photodynamic therapy

Oriol Penon,[a] María J. Marín,[*,b] David A. Russell,[b] Lluïsa Pérez-García,[*,a,1]

[a] Departament de Farmacologia, Toxicologia i Química Terapèutica and Institut de Nanociència i Nanotecnología UB (IN2UB), Universitat de Barcelona, Avda. Joan XXIII 27-31, 08028 Barcelona, Spain.

[b] School of Chemistry, University of East Anglia, Norwich Research Park, Norwich, Norfolk, NR4 7TJ, UK.

Corresponding Author

*E-mail: mlperez@ub.edu; M.Marin-Altaba@uea.ac.uk

[1] Present address: School of Pharmacy, The University of Nottingham, University Park, Nottingham NG72RD, England, UK.

## ABSTRACT

Photodynamic therapy (PDT) is a treatment of cancer by which tumour cells are destroyed using reactive oxygen species produced by photosensitisers following activation with visible or near infrared light. Successful PDT depends on the solubility and the targeting ability of the photosensitisers. In this work, the synthesis of a porphyrin-based water soluble nanoparticle conjugate containing a targeting agent that recognises the erbB2 receptor overexpressed on the surface of particular cancer cells is reported. The nanoparticle conjugates were synthesised following two different protocols, *viz.* a biphasic and a monophasic method, with the aim to determine which method yielded the optimal nanosystem for potential PDT applications. The nanoparticles were characterised using UV-Vis absorption and fluorescence spectroscopies together with transmission electron microscopy and zeta potential measurements; and their ability to produce singlet oxygen following irradiation was investigated following the decay in absorption of a singlet oxygen probe. The nanoparticles synthesised using the monophasic method were shown to produce the highest amount of singlet oxygen and were further functionalised with anti-erbB2 antibody to target the erbB2 receptors expressed on the surface of SK-BR-3 human breast cancer cells. The water soluble, antibody-porphyrin nanoparticle conjugates were shown to elicit targeted PDT of the breast cancer cells.

**Keywords:** Photodynamic therapy, Multifunctional nanoparticles, Porphyrins, Gold nanoparticles (AuNPs), Water soluble nanoconjugates, Targeting antibodies, Singlet oxygen production, *In vitro* phototoxicity, Human breast cancer cells

## INTRODUCTION

Photodynamic therapy (PDT) is an approach to cancer treatment based on the activation of photosensitiser drugs using visible or near infrared light to generate reactive oxygen species that induce cell death.[1] Characteristics such as: a high absorption coefficient and high photostability are required for a photosensitiser drug.[2] Examples of photosensitisers reported as effective for PDT treatment of cancer include organic molecules such as porphyrins, phthalocyanines and related tetrapyrroles.[3] One of the drawbacks of some of the reported photosensitisers when used as drugs for PDT is the non-specific distribution of the drug in the body, leading to possible side effects caused by the patient's exposure to sun light.[4] Furthermore, some of the currently used photosensitisers are hydrophobic molecules requiring their dispersion in emulsions or the use of delivery systems to administer the drugs. Such drawbacks of molecular photosensitisers for PDT can be overcome through the use of nanoparticles as drug delivery systems.[5] Silica nanoparticles,[6] polymeric nanoparticles,[7] magnetic nanoparticles,[5,7] quantum dots,[8] upconverting nanoparticles[9] and especially gold nanoparticles[5] are emerging as ideal candidates for use as delivery vehicles of hydrophobic photosensitisers for PDT. In the field of gold nanoparticles (AuNPs), Brust and co-workers reported a method based on the use of tetraoctylammonium bromide as the phase transfer reagent for the synthesis of gold nanoparticles functionalised with hydrophobic ligands that were ultimately soluble in polar solvents.[10] Following this method, Russell and co-workers reported phthalocyanine functionalised gold nanoparticles that were used for PDT of cancer and a higher production of singlet oxygen was observed for the bound photosensitiser when compared to the free drug.[11,12] Alternative procedures have been developed more recently for the synthesis of water soluble AuNPs functionalised with hydrophobic ligands.[5] These new synthetic methods

rely on the multifunctionalisation of the gold core, for example, by incorporating water soluble polymers or polyethyleneglycol (PEG) ligands to increase the water solubility of the nanosystem. Gamaleia *et al.* achieved the water solubility of gold nanoparticles functionalised with the porphyrin derivative hematoporphyrin by adsorbing the photosensitiser within a layer of polyvinylpyrrolidone that was used to stabilise the nanoparticle.[13] Another porphyrin derivative, protoporphyrin IX was reacted with a positively charged branched polyethyleneimine on the surface of gold nanoparticles yielding water stable nanostructures useful for PDT.[14] Zaruba *et al.* attached two porphyrin-brucine conjugates to 3-mercaptopropanoic acid modified gold nanoparticles (*ca.* 14.7 nm) yielding two types of porphyrin-stabilised nanoparticles that could be dispersed in culture media and that were tested for PDT both *in vitro* and *in vivo*.[15]

The use of PEG to provide water solubility to the nanoparticles has been applied by Burda and co-workers for the synthesis of gold nanoparticles containing a non-covalently bound silicon phthalocyanine.[16-19] PEG has also been used to provide water solubility and to enhance *in vivo* accumulation in the tumour tissue by the enhanced vascular permeability and retention effect of gold nanoparticles functionalised with a hydrophobic zinc phthalocyanine.[20] Furthermore, PEG can also be a key building block in the synthesis of nanosystems for targeted photodynamic therapy. Cancer cells that overexpress specific cell surface receptors can be selectively recognised by incorporating the corresponding targeting agents such as antibodies or lectins onto the surface of the nanoparticles. These specific antibodies or lectins can be linked to PEG functionalised nanoparticles *via* amide bond formation between the terminal carboxylic group of the PEG-derivative ligand and the amine residues present in the proteins. Russell and co-workers have reported targeted PDT of breast cancer cells using PEGylated gold nanoparticles functionalised with a phthalocyanine derivative ligand

and the antibody anti-erbB2 that recognizes the membrane receptor erbB2.[21] These authors have shown that the nanoparticle conjugates with the anti-erbB2 antibody selectively target the erbB2 receptor that is overexpressed on SK-BR-3 breast cancer cells while having limited or no targeted photoactivity for the MDA-MB-231 breast cancer cells (breast cancer cell line without erbB2 amplification) or normal mammary epithelial cells (MCF-10A). In addition, targeting of the T antigen on the surface of human colorectal adenocarcinoma cells has been achieved using the lectin Jacalin conjugated to phthalocyanine functionalised gold nanoparticles.[22,23]

Amongst the photosensitisers reported as useful for PDT,[3] porphyrins have been widely studied, especially since the development of the hematoporphyrin derivative, Photofrin®, that was first approved for the treatment of cancer in the 1990s and is currently used clinically.[3] We have recently reported the synthesis of a hydrophilic porphyrin that, when used to functionalise iron oxide nanoparticles, had potential applications as an agent for PDT;[24] and of water soluble gold nanoparticles functionalised with a thiolated porphyrin derivative and a thiolated PEG derivative that have demonstrated low intrinsic toxicity *in vitro* and are able to produce singlet oxygen in solution.[25] Thus, the use of water soluble porphyrin-coated gold nanoparticles in combination with antibodies covalently immobilised onto the nanoparticle surface could present a promising photosensitiser conjugate for targeted PDT.

Here, we report, to the best of our knowledge, the first multicomponent water soluble nanoparticle conjugate that combines the functionalisation of gold nanoparticles with a porphyrin derivative ligand, together with a PEG derivative ligand and an antibody targeting agent. First, gold nanoparticles functionalised with the porphyrin derivative containing an alkanethiol (5-[4-(11-mercaptoundecyloxy)phenyl]-10,15,20-triphenylporphyrin, **PR-SH**) and a thiolated carboxyl terminated PEG (**COOH-PEG-**

**SH**) were synthesised following two different protocols: 1) the biphasic method reported by Brust *et al.* using toluene and water;[10] and 2) a monophasic method that uses a mixture of dimethylformamide (DMF) and tetrahydrofuran (THF) as the solvent.[22] Both methods yielded water soluble nanoparticles (**PR-AuNP-PEG**, **Figure S1**) that were characterised by UV-Vis absorption spectroscopy, fluorescence spectroscopy, transmission electron microscopy and measuring their zeta potential. The photosensitiser surface coverage was investigated for both nanosystems to obtain the optimum water soluble functionalised nanoparticles potentially suitable for PDT. Since it was established that the nanoparticles **PR-AuNP-PEG**, produced *via* the monophasic method, contained more photosensitiser molecules on the nanoparticle surface and produced the highest amount of singlet oxygen, these nanoconjugates were chosen as the optimal nanosystem for potential PDT applications. An anti-erbB2 antibody to specifically target the erbB2 receptors overexpressed on the surface of SK-BR-3 breast cancer cells was incorporated onto the **PR-AuNP-PEG** (monophasic) yielding **PR-AuNP-PEG-Ab** nanoparticles (**Figure 1**) that proved successful for the production of singlet oxygen and induced cell death of the SK-BR-3 breast cancer cell following PDT irradiation.

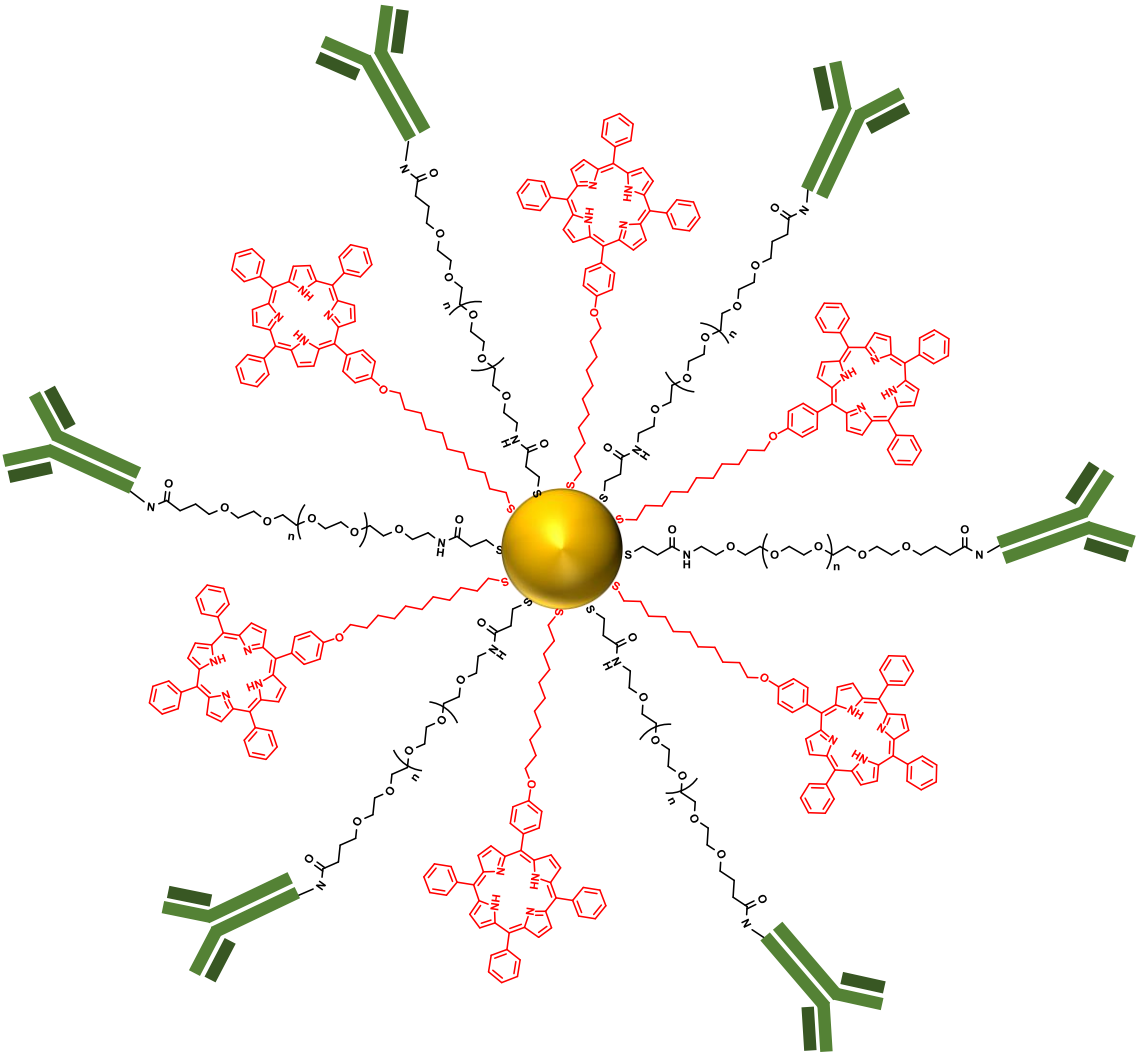

**Figure 1.** Schematic representation of the **PR-AuNP-PEG-Ab** conjugates: gold nanoparticles functionalised with the thiolated porphyrin derivative ligand (red) and the thiolated polyethylene glycol derivative ligand (black) bound to an anti-erbB2 antibody (green).

# EXPERIMENTAL PROCEDURES

## Materials and methods

Solvents: water, toluene, tetrahydrofuran (THF), *N*,*N*-dimethylformamide (DMF) methanol, propionic acid, ethyl acetate, hexane, distilled water, dichloromethane (DCM), chloroform, acetonitrile (ACN) and absolute ethanol were of analytical grade and used as received unless otherwise stated.

Commercially available compounds: pyrrole, *p*-hydroxybenzaldehyde, benzaldehyde, *S*-(11-bromoundecyl) thioacetate, potassium carbonate, gold(III) chloride trihydrate ($HAuCl_4 \cdot 3H_2O$), tetraoctylammonium bromide (TOAB), sodium borohydride ($NaBH_4$), *N*-hydroxysuccinimide (NHS), *N*-ethyl-*N*′-(3-dimethylaminopropyl) carbodiimide (EDC), 2-(*N*-morpholino)ethanesulfonic acid (MES) hydrate, propidium iodide and Tween 20 were purchased from Sigma-Aldrich, UK. α-Thio-ω-carboxy poly(ethylene glycol) 3073 Da (**COOH-PEG-SH**) was purchased from Iris Biotech GmbH. Anti-ErbB 2 antibody [ICR55] was purchased from Abcam, UK. 9,10-anthracenedipropionic acid (ADPA) was purchased from Molecular Probes. Sodium dihydrogen orthophosphate dihydrate ($NaH_2PO_4 \cdot 2H_2O$), di-sodium hydrogen orthophosphate anhydrous ($Na_2HPO_4$), sodium chloride (NaCl), phosphate buffered saline (PBS) tablets, foetal bovine serum, 75 $cm^3$ Nunc Easy tissue culture flasks with porous caps, Nunc multidishes and 18 mm diameter glass coverslips were purchased from Thermo Fisher Scientific, UK. Sodium hydrogen carbonate ($NaHCO_3$) was purchased from BDH Laboratory Supplies Poole, UK. Trypsin 0.25 % (1x) with ethylenediaminetetraacetic acid (EDTA), L-glutamine and McCOY's 5A medium were purchased from Invitrogen, UK. Millex GP syringe driven filter units (0.22 μm) were purchased from Millipore Corporation, USA. Sterile centrifuge tubes and sterile

disposable serological pipettes, individually wrapped, were purchased from Corning B. V. Life Sciences (The Netherlands). Vivaspin™ 500 µL columns (100 KDa molecular weight cut off, with polyethersulfone membrane) were purchased from Sartorius Biotech, UK.

SK-BR-3 human breast adenocarcinoma cells were purchased from LGC Standards. The SK-BR-3 cell line was kindly provided by Prof Dylan R. Edwards (School of Biological Sciences, University of East Anglia, UK).

## Instrumental techniques

UV-Vis absorption spectra were recorded using a Hitachi U-3000 spectrophotometer, using quartz cuvettes with a 1 cm path length. Fluorescence excitation and emission spectra were recorded using a Hitachi F-4500 fluorescence spectrometer. The fluorescence excitation and emission spectra were recorded using quartz cuvettes with a 1 cm path length. Transmission electron microscopy (TEM) images were obtained using a Jeol 2000EX TEM operating at 200 kV. Samples (5 µL) were deposited on a holey carbon film 300 mesh copper grids from Agar Scientific, UK. Zeta potential measurements were recorded using a Malvern Zetasizer Nano-ZS. Centrifugation of the nanoparticles was performed using a Beckman Coulter Allegra™ X-22R centrifuge. SK-BR-3 cells were imaged using a Zeiss Axiovert 200M microscope. Fluorescence images were captured using a 63x PlanApochromat (1.4 NA) oil-immersion objective lens, a Zeiss AxioCam MRm CCD camera and AxioVision software. Images collected were processed using the AxioVision SE64 Rel. 4.8 software.

## Synthetic protocols

*Synthesis of the thiolated porphyrin derivative ligand **PR-SH***

The thiolated porphyrin derivative ligand, 5-[4-(11-mercaptoundecyloxy)phenyl]-10,15,20-triphenylporphyrin (**PR-SH**) was synthesised following a protocol recently reported by our group.[25]

*Synthesis of the water soluble functionalised nanoparticles (**PR-AuNP-PEG**)*

***Method A:*** This method was based on a protocol previously reported by Brust *et al.*[10] A solution of $HAuCl_4 \cdot 3H_2O$ (3.6 mg, 9.14 µmol) in water (0.5 mL) was added to a stirred solution of tetraoctylammonium bromide (11 mg, 20.14 µmol) in toluene (1 mL). **PR-SH** (2 mg, 2.44 µmol) and **COOH-PEG-SH** (7.5 mg, 2.44 µmol) were dissolved in toluene (0.5 mL) and the solution was then added to the aqueous gold solution. An excess of $NaBH_4$ (5.3 mg, 0.14 mmol) in water (1 mL) was added dropwise to the mixture. The mixture was reacted overnight under continuous stirring at room temperature. The aqueous phase of the resulting dark red solution was separated from the organic phase using an extraction funnel. The water was removed by rotary evaporation and the solid was washed with ethanol (3 x 5 mL) using centrifugation (13,000 rpm, 30 min). The resulting **PR-AuNP-PEG** (biphasic) were stored at 4 °C in MES buffer (50 mM, pH 5.5, 0.05% Tween 20).

***Method B:*** This method was based on a protocol previously reported by Obaid *et al.*[22] **PR-SH** (1 mg, 1.22 µmol) was dissolved in dry THF (0.5 mL) and was added to a stirred solution of the **COOH-PEG-SH** (3.75 mg, 1.22 µmol) in dry THF (1 mL). After 5 min, a solution of $HAuCl_4 \cdot 3H_2O$ (0.6 mg, 1.52 µmol) in dry DMF (0.6 mL) was added. The reaction was stirred for 5 min and a fresh solution of $NaBH_4$ (0.75 mg, 19.8 µmol) in DMF (0.6 mL) was rapidly added. The reaction was stirred overnight at room

temperature. Next, THF (4 mL) was added and the solution was centrifuged (5,000 rpm, 2 min). The gold nanoparticles functionalised with both ligands, **PR-SH** and **COOH-PEG-SH**, remained stable in the THF while any gold nanoparticles not functionalised with the **PR-SH** ligand precipitated. The supernatant was collected and the solvent was removed by rotary evaporation. THF (4 mL) was added and the solution was centrifuged (5,000 rpm, 2 min) to remove the gold nanoparticles non-functionalised with **PR-SH**, which stay in the pellet. The supernatant was collected and the solvent evaporated by rotary evaporation. The solid obtained was dissolved in 5 mL of MES buffer (50 mM, pH 5.5, 0.05% Tween 20). Finally, the solution was centrifuged (13,000 rpm, 30 min) and the supernatant containing the **PR-AuNP-PEG** (monophasic) were stored at 4 °C.

*Synthesis of the non-water soluble porphyrin functionalised nanoparticles (**PR-AuNP**)*

A solution of $HAuCl_4 \cdot 3H_2O$ (3 mg, 7.6 µmol) in water (5 mL) was added to a stirred solution of tetraoctylammonium bromide (7.6 mg, 13.8 µmol) in toluene (5 mL). **PR-SH** (5 mg, 6.1 µmol) was dissolved in toluene (1.5 mL) and added to the biphasic solution. An excess of $NaBH_4$ (5.3 mg, 0.140 mmol) in water (1 mL) was slowly added to the mixture. The reaction was stirred at room temperature overnight. The organic phase of the resulting dark red solution was separated using an extraction funnel and then the solvent was removed by rotary evaporation. The solid sample was washed with ethanol (3 x 5 mL), which each washing removed by centrifugation (13,000 rpm, 30 min) to give **PR-AuNP** as a red solid that was soluble in DCM or DMSO.

*Synthesis of the antibody functionalised nanoparticles (**PR-AuNP-PEG-Ab**)*

*N*-ethyl-*N*′-(3-dimethylaminopropyl) carbodiimide (EDC, 0.4 µL, 2.25 µmol) and *N*-hydroxysuccinimide (NHS, 1.5 mg, 13 µmol) were added to 1 mL of the **PR-AuNP-PEG** (monophasic) solution and the mixture was stirred at room temperature for 30

min. Excess EDC and NHS were removed by centrifugation (14,000 rpm for 30 min at 4 °C) using Vivaspin$^{TM}$ 500 µL columns. The nanoparticles were resuspended in PBS buffer (1 mL, pH 7.4) and anti-ErbB2 antibody (18 µL, 1 mg/mL) was added. The mixture was stirred slowly for 15 h at room temperature. Finally, the unbound antibody was removed from the nanoparticle solution by five repeated filtrations of the sample in Vivaspin$^{TM}$ 500 µL columns (14,000 rpm, 30 min at 4 °C). After each centrifugation, the nanoparticles were resuspended in 500 µL of PBS, yielding **PR-AuNP-PEG-Ab** that were kept in sterilised PBS at 4 °C.

## Singlet oxygen production

ADPA reacts with singlet oxygen to give an endoperoxide, the formation of which can be observed by UV-Vis absorption spectroscopy.[26] ADPA (50 µL of a 1.1 mM solution in methanol) was added to 550 µL of the **PR-SH** in DCM, **PR-AuNP** in DMSO, and **PR-AuNP-PEG** (biphasic), **PR-AuNP-PEG** (monophasic) and **PR-AuNP-PEG-Ab** in PBS buffer. The solutions were added to a quartz cuvette and stirred thoroughly. A blue light source, with a wavelength range between 400 and 500 nm, was used to irradiate the solutions during 4 h under stirring. An UV-Vis absorption spectrum between 300 and 700 nm of each sample was recorded every hour, and the singlet oxygen production was determined by the decrease of the absorption intensity at 378 nm of the ADPA.

## Biological experiments

*Imaging medium*

The imaging medium based on Hank's balanced salt solution (HBSS) was prepared in water containing NaCl (120 mM), KCl (5 mM), $CaCl_2$ (2 mM), $MgCl_2$ (1 mM), $NaH_2PO_4 \cdot 2H_2O$ (1 mM), $NaHCO_3$ (1 mM) and 4-(2-hydroxyethyl)piperazine-4-ethanesulfonic acid (HEPES, 25 mM). The pH of the imaging medium was adjusted to pH 7.2 using aqueous solutions of NaOH and HCl (0.01 – 1.00 M). The imaging medium was supplemented with bovine serum albumin (1 mg/mL), basal medium eagle amino acids (2%), glutamine (2 mM) and glucose (11 mM). The imaging medium was sterilised by filtration through a Millex GP syringe driven filter unit (0.22 μm) prior to use.

*Phosphate buffer saline (PBS)*

The phosphate buffered saline solution used for the cell-based experiments was prepared by dissolving 10 PBS tablets in water (1 L). This solution was sterilised by autoclaving at 110 °C for 10 min. The as-prepared PBS solutions contained $Na_2HPO_4$ (8 mM), $KH_2PO_4$ (1 mM), NaCl (160 mM), and KCl (3 mM); and had a pH value of 7.3.

The PBS buffer (10 mM) used to dissolve the propidium iodide was prepared using $NaH_2PO_4 \cdot 2H_2O$ and $Na_2HPO_4$ stock solutions (200 mM). The as-prepared PBS solutions contained NaCl (150 mM) and calcium chloride dihydrate (100 μM). The pH of the PBS was adjusted to pH 7.4 using aqueous solutions of NaOH and HCl (0.01 – 1.00 M). The buffer was sterilised by filtration through a Millex GP syringe driven filter unit (0.22 μm) prior to use.

*SK-BR-3 cell culture*

SK-BR-3 human breast adenocarcinoma cells were cultured in McCOY's 5A medium supplemented with 10% foetal bovine serum and 1.5% L-glutamine (200 mM). The cells were routinely cultured at 37 °C in a 5% $CO_2$ atmosphere in 75 $cm^3$ Nunc Easy tissue culture flasks with porous caps. Subcultures (1:6) were made every 5 days by washing the cells with PBS and dislodging the cells from the flask surface using trypsin 0.25% (1x) EDTA.

*Culture of SK-BR-3 cells onto coverslips*

For imaging, SK-BR-3 cells were cultured on 18 mm diameter glass coverslips 22 – 24 h prior to performing imaging experiments. Cells were cultured at 37 °C in a 5% $CO_2$ atmosphere in a 75 $cm^3$ tissue culture flask until they reached near confluence. Cells were washed with PBS and harvested from the flask using trypsin as indicated previously. A sterile coverslip was placed in each well of a 6-well Nunc multidish. Supplemented McCOY's medium (2 mL) and an aliquot of the cell suspension (1 mL) were added to each well covering the coverslip. The cells were then incubated at 37 °C in a 5% $CO_2$ atmosphere for 22 – 24 h.

*Incubation of SK-BR-3 cells with **PR-AuNP-PEG-Ab***

The growth medium in the well containing the coverslip with the SK-BR-3 cells of interest was removed using a pipette. The cells were washed once with PBS (1 mL) and incubated for 3 h at 37 °C in a 5% $CO_2$ atmosphere in McCOY's medium supplemented only with L-glutamine (1.5 mM) containing **PR-AuNP-PEG-Ab** (0.8 μM porphyrin equivalent).

SK-BR-3 control cells were grown in a similar manner but without the **PR-AuNP-PEG-Ab** conjugates.

*Incubation of SK-BR-3 with propidium iodide*

Propidium iodide (5 µL, 1 mg/mL in PBS) was mixed with HBSS-based imaging medium (1 mL), this was added to stain the SK-BR-3 cells on the coverslip and incubated in the dark at 37 °C.

*Imaging and irradiation of SK-BR-3 cells loaded with and without **PR-AuNP-PEG-Ab***

For imaging, 18-mm cover slips containing the SK-BR-3 cells were placed in a Ludin chamber (Life Imaging Service, Olten, Switzerland) which was securely tightened. Each coverslip was washed three times with HBSS-based imaging medium and the Ludin chamber was mounted on a stage at 37 °C in a Zeiss Axiovert 200M microscope. The images were acquired with a 63x PlanApochromat (1.4 NA) oil-immersion objective. The **PR-AuNP-PEG-Ab** uptaken by the cells were excited at 530 – 585 nm and the fluorescence emission was collected through a 600 nm long-pass filter. To activate the generation of singlet oxygen by the **PR-AuNP-PEG-Ab** within the cells, the cells were illuminated through the objective with the light from a mercury arc lamp reflected off a long-pass, dichroic mirror with a cut-off of 495 nm for 30 s.

*Imaging of SK-BR-3 cells loaded with propidium iodide*

The propidium iodide stained the nucleus of dead cells with significant membrane damage. Fluorescence from the propidium iodide was excited at 530-585 nm and the fluorescence emission collected through a 600 nm long-pass filter.

## RESULTS AND DISCUSSION

### Synthesis of the functionalised nanoparticles: PR-AuNP-PEG and PR-AuNP

The synthesis of the thiolated porphyrin derivative ligand, 5-[4-(11-mercaptoundecyloxy)phenyl]-10,15,20-triphenylporphyrin (**PR-SH**), was accomplished following a previously reported protocol.[25] The ligand **PR-SH** was used, together with the α-thio-ω-carboxy-polyethylene glycol derivative ligand (**COOH-PEG-SH**) for the functionalisation of gold nanoparticles. Both ligands are suitable to functionalise gold nanoparticles through the presence of the thiol groups. The function of the porphyrin derivative on the nanoparticles is to act as the photosensitiser to produce singlet oxygen. The PEG derivative ligand has a double function: 1) to increase the water solubility of the nanoparticles and 2) to immobilise the targeting antibody anti-erbB2 through the terminal carboxylic group. The functionalisation of the AuNP with **PR-SH** and with **COOH-PEG-SH** to generate **PR-AuNP-PEG** was achieved following two different approaches:

- In *Method A*, based on the biphasic method previously described by Brust *et al.*,[10] **PR-SH** was dissolved in toluene and mixed with **COOH-PEG-SH** and the metallic gold precursor ($HAuCl_4$) dissolved in water. Tetraoctylammonium bromide (TOAB) was added as the phase transfer agent and $NaBH_4$ as the reducing agent, and the mixture was reacted overnight to obtain the water soluble **PR-AuNP-PEG** (biphasic) nanoparticles (**Figure S1**).
- In *Method B*, based on a monophasic method,[22] the reaction occurs only in one phase since **PR-SH** and **COOH-PEG-SH** are both dissolved in THF and mixed with a solution of $HAuCl_4$ in DMF to which a solution of $NaBH_4$ also in DMF is

added. THF and DMF are miscible solvents providing a unique reaction phase. The mixture was left stirring overnight to obtain the water soluble **PR-AuNP-PEG** (monophasic) nanoparticles (**Figure S1**).

The properties of the nanoparticles obtained following both methods were compared in order to determine the optimal nanoparticles in terms of size, distribution, photosensitiser coverage and ability to produce singlet oxygen.

Additionally, gold nanoparticles coated only with the porphyrin derivative ligand **PR-SH** (**PR-AuNP** – **Figure S2**) were synthesised using the biphasic method and were soluble in DCM and DMSO, and their properties were compared with those of the **PR-AuNP-PEG** nanoparticles.

Noticeably, the method of synthesis has a clear influence not only on the size of the formed nanoparticles but, importantly, on their chemical composition (see later). This could be the result of two aspects which are worth noting: a) The amount of **PR-SH** varies according to the methodology used, since less porphyrin (relative to gold) is used for the biphasic synthesis; thus, the ratio **Au:PR-SH** for **PR-AuNP-PEG** (monophasic) is 1:1, whereas for **PR-AuNP-PEG** (biphasic) is 3.7:1, and for **PR-AuNP** is 1.2:1. b) The biphasic methodology follows different kinetics, since it involves initial encapsulation, phase transfer and stabilization of the gold by the surfactant TOAB, followed by surface exchange with a thiol ligand (e.g. **PR-SH**), whereas the monophasic system allows direct linkage of the thiolated species to the growing gold surface of the nanoparticle.

## Characterisation of the functionalised nanoparticles.

### UV-Vis extinction spectroscopy

UV-Vis extinction spectroscopy was used to characterise the different synthesised gold nanoparticles and to confirm their functionalisation with the porphyrin derivative ligand **PR-SH** (**Figure 2**). The UV-Vis absorption spectrum of the free ligand **PR-SH** exhibited the Soret band at $\lambda$ = 422 nm and the four Q bands between 500 and 700 nm characteristic of metal free porphyrin derivatives.[27] The characteristic Soret band was also observed in the UV-Vis extinction spectra of the synthesised nanoparticles, **PR-AuNP** and **PR-AuNP-PEG**, albeit slightly shifted from that of the free ligand, at *ca.* 419 nm for **PR-AuNP**, 425 nm for **PR-AuNP-PEG** (monophasic) and 429 nm for **PR-AuNP-PEG** (biphasic), respectively. The presence of the Soret band in the UV-Vis extinction spectrum of the nanoparticles confirmed the functionalisation of the gold core with the porphyrin derivative ligand for all of the nanoparticles synthesised. The slight red-shift in the position of this characteristic absorption band of the porphyrin could be attributed to the different environment in which **PR-SH** ligand is found when attached to the gold nanoparticles, indicating the formation of a weakly coupled J-aggregate.

The UV-Vis extinction spectra of **PR-AuNP-PEG** (monophasic) and **PR-AuNP** also exhibited the characteristic four Q bands of the porphyrin between 500 and 700 nm although the absorption bands were broader and less intense than those observed in the UV-Vis absorption spectrum of the free **PR-SH**.

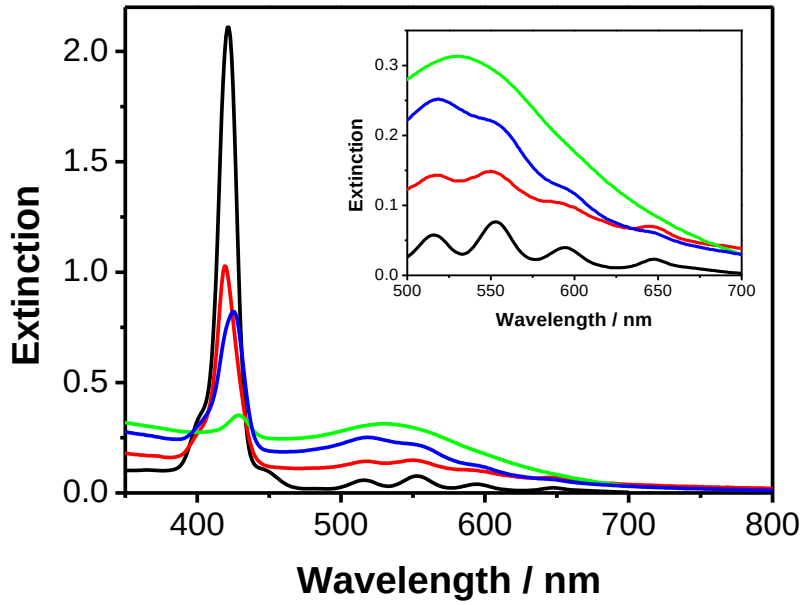


**Figure 2.** UV-Vis extinction spectrum of the free **PR-SH** ($2.04 \cdot 10^{-4}$ mg/mL, black) and **PR-AuNP** (0.4 mg/mL, red) in DCM; **PR-AuNP-PEG** (biphasic) (green) and **PR-AuNP-PEG** (monophasic) (blue) in MES buffer (0.4 mg/mL). Inset: Magnification of the Q band region from 500 to 700 nm.

## Transmission electron microscopy

The functionalised nanoparticles were characterised using transmission electron microscopy (TEM) to determine their morphology, polydispersity and size (**Figure 3**). The **PR-AuNP-PEG** nanoparticles were spherical in shape with low polydispersity and uniform size distribution with mean diameters of *ca.* 4.5 nm and 9 nm, for the biphasic and monophasic synthetic methods, respectively, as shown in the histograms of **Figure 3b** and **3d**. These results show that the functionalised nanoparticles synthesised using the biphasic method were smaller than those synthesised using the monophasic method with a mixture of DMF/THF as the solvent. **PR-AuNP**, synthesised using the biphasic

method had, as expected, a similar size (diameter *ca*. 5 nm) and shape than the **PR-AuNP-PEG** (biphasic) (**Figure S3**).

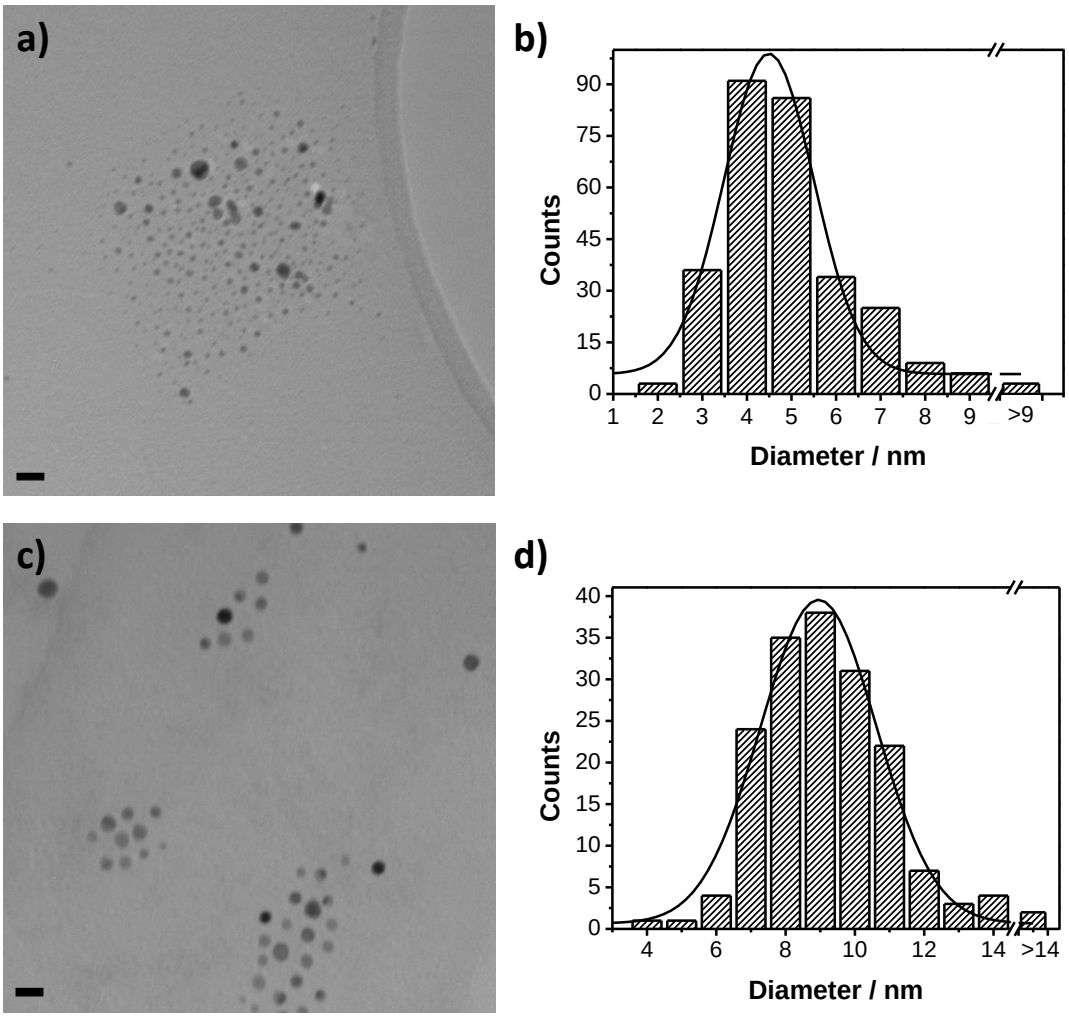


**Figure 3.** Transmission electron micrographs (**a** and **c**) and size distribution histograms (**b** and **d**) of: **a** and **b) PR-AuNP-PEG** (biphasic) (n = 298) and **c** and **d) PR-AuNP-PEG** (monophasic) (n = 172). Scale bars: 20 nm.

## Quantification of the porphyrin derivative ligand on the surface of the nanoparticles

Quantifying the amount of photosensitiser molecules that are self-assembled on the surface of the AuNPs is relevant since this concentration would be related to the quantity of singlet oxygen that the functionalised nanoparticles can produce. The number of **PR-SH** molecules immobilised on the surface of AuNPs can be estimated by UV-Vis absorption spectroscopy using the absorption intensity of its Soret band. First, a calibration curve using known concentrations of **PR-SH** in DCM solution (from 0.5 to 15 µM) was obtained (**Figure S4**). From the calibration curve, the extinction coefficient of **PR-SH** was estimated to be $\varepsilon_{418nm} = 3.75x10^4\ M^{-1}\cdot cm^{-1}$. Applying the Beer-Lambert law and the calibration curve given in **Figure S4**, the concentration of the **PR-SH** immobilised on the different synthesised gold nanoparticles can be estimated. To eliminate the contribution of the gold nanoparticles to the UV-Vis extinction spectrum of the functionalised nanoparticles, the extinction at 460 nm (contribution of the AuNPs) was subtracted from the corresponding Soret band of the porphyrin (*ca.* 430 nm, 426 nm and 418 nm for **PR-AuNP-PEG** (biphasic), **PR-AuNP-PEG** (monophasic) and **PR-AuNPs**, respectively) as indicated in **Figure S5**. Concentrations of **PR-SH** of 2.55 µM, 16.65 µM and 41.43 µM were estimated for **PR-AuNP-PEG** (biphasic), **PR-AuNP-PEG** (monophasic) and **PR-AuNPs**, respectively (see **Figure S6** for calculations). These results indicate that **PR-AuNP-PEG** synthesised using the monophasic method have a considerably larger concentration of porphyrin molecules on the particle surface than the **PR-AuNP-PEG** (biphasic). As expected, the highest number of porphyrin molecules were present on the surface of the **PR-AuNPs**.

Once the concentration of **PR-SH** for each type of nanoparticles and their respective diameters are known, the ratios of porphyrin per nanoparticle can be estimated using the

calculations reported by Haiss *et al*.[28] The ratio of porphyrin per nanoparticle was determined to be 56 for **PR-AuNP-PEG** (biphasic) and 3882 for **PR-AuNP-PEG** (monophasic) (**Table 1**). These results clearly show that using the monophasic synthesis methodology the quantity of immobilised **PR-SH** was *ca.* 69 times higher than when the biphasic methodology was used. The same approach was followed to calculate the ratio of porphyrin/AuNPs on the non-water soluble **PR-AuNPs**, obtaining 678 porphyrins per nanoparticle (**Table 1**). The ratio of porphyrin present per $nm^2$ of nanoparticle was calculated using the corresponding estimated porphyrin/AuNP ratios and calculating the area of each type of spherical surface AuNPs (**Table 1**). The number of porphyrin molecules per $nm^2$ was estimated to be 15.26 for **PR-AuNP-PEG** (monophasic), 0.88 for **PR-AuNP-PEG** (biphasic), and 8.64 for **PR-AuNP**.

These results confirm that the methodology of synthesis is crucial for the size and composition of the AuNPs. One phase synthesis, which uses a ratio of **PR-SH** relative to gold (1:1) and a different diffusion and coating kinetics in the continuous phase, leads to functionalised particles that are bigger (diameter *ca*. 9 nm) and have a higher content of **PR-SH** (**Table 1**). Two phase synthesis gives smaller nanoparticles (*ca*. 5 nm diameter) and less enriched in **PR-SH**, especially for **PR-AuNP-PEG** (biphasic), where two thiol ligands (**PR-SH** and **COOH-PEG-SH**) compete for the gold surface.

**Table 1.** Estimated values of: 1) the concentration of immobilised **PR-SH**, 2) the number of molecules of **PR-SH** per AuNP, 3) diameter of the different types of AuNPs (nm), 4) the surface area per AuNP, and 5) the ratio porphyrin derivative ligand per AuNP.

| | *Immobilised* ***PR-SH*** | *Ratio* **PR-SH** */AuNP* | *AuNP diameter (nm)*[a] | *AuNP area (nm$^2$)* | *Ratio* **PR-SH** */AuNP area (nm$^2$)*[b] |
|---|---|---|---|---|---|
| ***PR-AuNP-PEG (biphasic)*** | 2.55 µM | 56 | 4.5 | 63.6 | 0.88 |
| ***PR-AuNP-PEG (monophasic)*** | 16.65 µM | 3882 | 9 | 254.4 | 15.26 |
| ***PR-AuNP*** | 41.43 µM | 678 | 5 | 78.5 | 8.64 |

[a]Measured by TEM. [b]Number of **PR-SH** molecules per nm$^2$ of nanoparticle surface.

## Fluorescence spectroscopy

The porphyrin functionalised gold nanoparticles were further characterised using fluorescence spectroscopy. **Figure 4** shows the fluorescence emission spectra of the free ligand **PR-SH** and of the different porphyrin functionalised gold nanoparticles in solution. The fluorescence emission spectrum of the free **PR-SH** exhibits two emission bands at λ *ca.* 650 and 712 nm that are characteristic of porphyrin derivatives.[27] The two characteristic bands were also observed for the **PR-AuNP-PEG** (monophasic) and for **PR-AuNP**; however, they were not present in the fluorescence emission spectrum of the **PR-AuNP-PEG** (biphasic) possibly due to the low concentration of **PR-SH** on the surface of these nanoparticles. The fluorescence excitation spectra of the free ligand **PR-SH** and of the functionalised nanoparticles were also obtained (**Figure S7**). Again, the characteristic porphyrin excitation spectrum was only observed for the **PR-SH**, **PR-AuNP-PEG** (monophasic) and **PR-AuNP**.

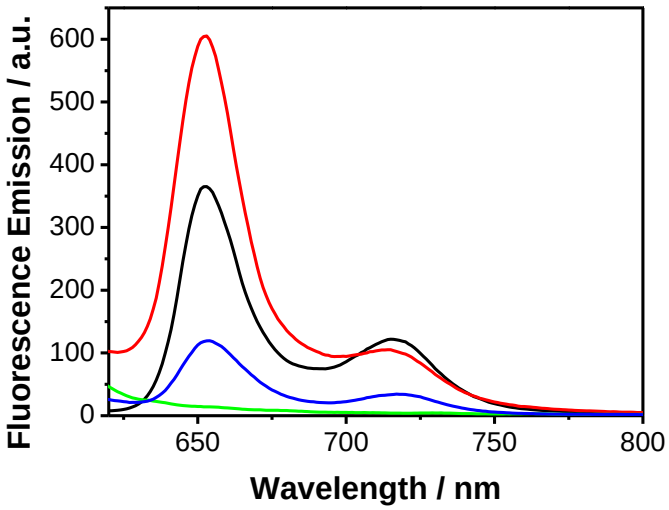


**Figure 4**. Fluorescence emission spectra (excitation at λ = 591 nm) of: **PR-SH** ($2.04 \cdot 10^{-4}$ mg/mL in DCM – black), **PR-AuNP-PEG** (biphasic) (0.4 mg/mL in water – green), **PR-AuNP-PEG** (monophasic) (0.4 mg/mL in water – blue) and **PR-AuNP** (0.4 mg/mL in DCM – red). The spectrum of the free ligand **PR-SH** was recorded using ex/em slits = 5 while the spectra of the porphyrin functionalised gold nanoparticles were recorded using ex/em slits = 10.

The different techniques used to characterise the porphyrin functionalised gold nanoparticles confirmed that the **PR-AuNP-PEG** (monophasic) incorporated a larger number of the **PR-SH** ligands on the nanoparticle's surface than those produced using the biphasic synthetic method. Also, **PR-AuNPs** incorporate a high number of **PR-SH**; however, they are not water soluble and they do not have any functional moieties to enable the incorporation of an antibody onto the nanostructure. **PR-AuNP-PEG** contain terminal carboxylic acid groups, at the end of the PEG ligand, capable of forming covalent bonds with biomolecules such as antibodies. Therefore, the water soluble **PR-AuNP-PEG** (monophasic) were chosen as the more promising nanoparticles for the production of singlet oxygen and the incorporation of targeting antibodies.

## Antibody anti-erbB2 immobilisation: synthesis and characterization of PR-AuNP-PEG-Ab conjugates

To achieve an active targeting of cancer cells, anti-erbB2 antibodies were immobilised on the surface of the **PR-AuNP-PEG** (monophasic) since these water soluble nanoparticles contained the highest concentration of photosensitiser molecules. The antibody anti-erbB2 was chosen since it recognizes selectively the erbB2 receptors that are overexpressed on the cellular surface of *ca.* 25% of breast cancers.[29] The antibody anti-erbB2 was linked to the terminal carboxylic groups of the PEG ligands as shown in **Figure 1**. The carboxylic groups of the PEG ligands were first activated by EDC/NHS chemistry to form stable amide bonds with the antibody yielding **PR-AuNP-PEG-Ab** conjugates. The UV-Vis extinction spectrum of the **PR-AuNP-PEG-Ab** conjugates exhibited the characteristic bands of the porphyrin derivative ligand and a band at *ca.* 280 nm characteristic of the protein structure[30] (**Figure S8**), thus confirming the functionalisation of the nanoparticles with the anti-erbB2 antibody.

The charge on the surface of the synthesised nanoparticles, which depends on the coating surrounding the nanocore, was analysed by measuring the zeta potential of the different samples (**Table S1**). Both **PR-AuNP-PEG** nanoparticles, biphasic and monophasic, have a negative zeta potential since the terminal carboxylic groups of the PEG ligands are negatively charged at neutral pH (PBS, pH 7.4). The difference in the zeta potential value between the **PR-AuNP-PEG** (biphasic) (-21.96 mV) and **PR-AuNP-PEG** (monophasic) (-11.76 mV) suggests that the former are coated with a greater amount of PEG ligands. Following immobilisation of the antibody, the zeta potential of the **PR-AuNP-PEG** (monophasic) increased to 0.04 mV. This could be due to the formation of amide bonds between the terminal carboxylic group in the PEG ligands and the amines in the anti-erbB2 antibodies.

## Singlet oxygen production

The ability of the free ligand **PR-SH** and of the functionalised nanoparticles to produce singlet oxygen was investigated. The different samples were irradiated during 4 h with a blue light source (λ = 400-500 nm) in the presence of 9,10-anthracenedipropionic acid (ADPA), a singlet oxygen probe. ADPA undergoes a continuous photobleaching in the presence of singlet oxygen due to the formation of an endoperoxide.[26] The formation of the endoperoxide can be followed by measuring the UV-Vis absorption decay of the ADPA upon irradiation.

The photobleaching of the ADPA upon irradiation of **PR-SH** and of the **PR-AuNP** with a blue light source is shown in **Figure S9** (**a** and **b**, respectively). These experiments were performed in DCM since both **PR-SH** and **PR-AuNP** are not water soluble. The absorption band observed at *ca.* 420 nm corresponds to the Soret band of the porphyrin derivative whereas the bands at *ca.* 400, 378, 360 and 340 nm correspond to the characteristic absorbance profile of the ADPA molecule. The decay of the ADPA absorption was observed for both samples, indicating the formation of the endoperoxide and therefore, the production of singlet oxygen. A decrease in the Soret band was also observed for the **PR-AuNP**, possibly due to partial decomposition of the porphyrin during the formation of the singlet oxygen.

**Figure S9** (**c** and **d**) show the time-dependent decay of the ADPA absorption spectrum following irradiation of the water dispersible nanoparticles **PR-AuNP-PEG** (biphasic) and **PR-AuNP-PEG** (monophasic), respectively. It was observed that the decay of the absorption of ADPA was higher for the **PR-AuNP-PEG** (monophasic) than for the **PR-AuNP-PEG** (biphasic), as expected due to the higher concentration of porphyrin derivative ligand on the nanoparticle's surface. No significant changes were

observed with the Soret band of these two types of functionalised nanoparticles. The same experiment was performed with the **PR-AuNP-PEG-Ab** conjugates to investigate whether the presence of the antibody had any effect on the singlet oxygen production (**Figure S9e**). Photobleaching of ADPA was also observed when the **PR-AuNP-PEG-Ab** conjugates were irradiated for 4 hours, thus confirming the production of singlet oxygen by the antibody functionalised nanoparticles.

A summary of the progressive decay of the ADPA absorption band at λ = 378 nm upon irradiation of the free porphyrin **PR-SH** and the four different porphyrin functionalised gold nanoparticles is shown in **Figure S10**, indicating the percentage of the ADPA that had been converted to the endoperoxide. After 4 hours following irradiation of the samples, the levels of ADPA decay for **PR-SH**, **PR-AuNP**, **PR-AuNP-PEG** (monophasic) and **PR-AuNP-PEG-Ab** were 43%, 20%, 24% and 14%, respectively. These results indicate that these four samples produce singlet oxygen following irradiation. However, the ADPA decay upon irradiation of **PR-AuNP-PEG** (biphasic) was just 2% indicating a low singlet oxygen production by these functionalised nanoparticles. This latter result was to be expected with the low concentration of photosensitiser on the nanoparticle's surface.

To be able to compare the singlet oxygen production of the different samples, the maximum rate of ADPA photobleaching was normalised using the corresponding concentration of the photosensitiser and following **Equation 1**.

$$\%\, rate\ of\ \ ADPA\ Photobleaching = \frac{(\%Abs_{378}\ at\ t = 0\,\text{min}) - (\%Abs_{378}\ at\ t = 60\,\text{min})}{60\,\text{min} \times [\,phorphyrin](mM)}$$

**Equation 1**. Equation used to calculate the maximum rate of ADPA photobleaching.

The calculated % rates of ADPA photobleaching for the five analysed samples are shown in **Figure 5**. **PR-AuNP-PEG** (monophasic) (% rate of ADPA photobleaching of 5.5% Abs/(min·mM)) produce singlet oxygen in a more efficient manner than **PR-AuNP-PEG** (biphasic) (2.1% Abs/(min·mM)). These results confirm that the nanoparticles containing more porphyrin derivative ligands per nanoparticle (**PR-AuNP-PEG** (monophasic)) produce a greater amount of singlet oxygen. The calculated % rate of ADPA photobleaching for **PR-SH** was 1.6% Abs/(min·mM), while the **PR-AuNP** showed the highest % rate of ADPA photobleaching (9% Abs/(min·mM)). This last observation also clearly indicates the enhancement in singlet oxygen production induced by the immobilisation of **PRSH** onto the nanoparticles. The % rate of ADPA photobleaching for **PR-AuNP-PEG-Ab** conjugates, 2.3% Abs/(min·mM), was a similar result to that of **PR-AuNP-PEG** (monophasic). Overall, these results demonstrate that: 1) when the porphyrin is immobilised onto the surface of the gold nanoparticles, singlet oxygen is produced, 2) the % rate of ADPA photobleaching achieved is proportional to the amount of porphyrin on the nanoparticles, 3) the solvent has a pronounced influence on the singlet oxygen quantification, probably due to the reduced lifetime of singlet oxygen in aqueous solutions as compared to that found in organic solvents,[31] and 4) the presence of the antibody appears to affect slightly the singlet oxygen production of the porphyrin functionalised nanoparticles, making **PR-AuNP-PEG-Ab** moderately less efficient. However, the variation in singlet oxygen production in the presence of the antibody is small.

Although **PR-AuNP** showed the highest % ADPA photobleaching, **PR-AuNP-PEG** (monophasic) provide a nanoparticle formulation suitable for the incorporation of the anti-erbB2 antibody giving **PR-AuNP-PEG-Ab** that are still active for single oxygen

production and at the same time should be target selective, providing the best candidate for *in vitro* PDT experiments.

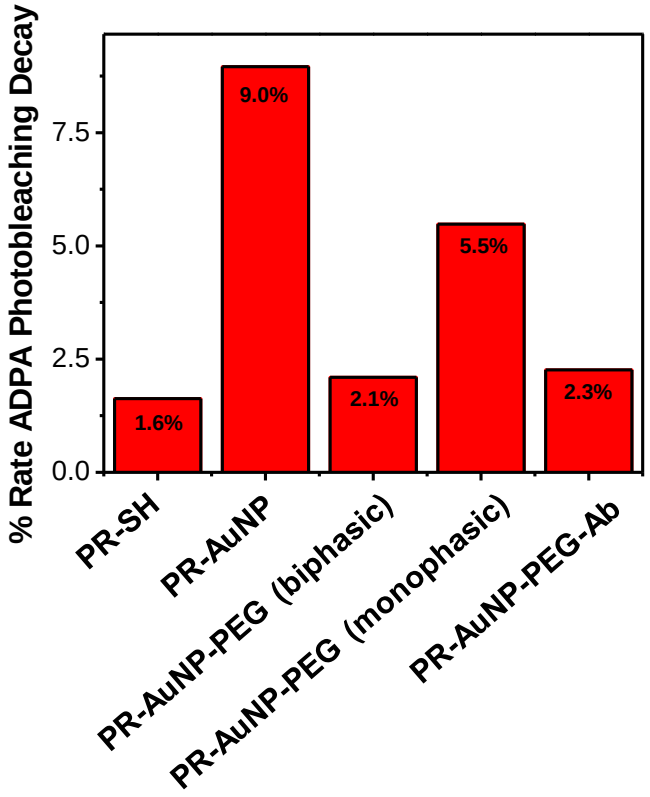


**Figure 5.** Percentage rate of ADPA photobleaching of the porphyrin derivative ligand **PR-SH** and of the four different functionalised gold nanoparticles calculated based on the concentration of photosensitiser on the particles.

## *In vitro* PDT experiments using SK-BR-3 breast cancer cells

To determine the suitability of the **PR-AuNP-PEG-Ab** conjugates for PDT, *in vitro* studies using a SK-BR-3 breast cancer cell line were performed. SK-BR-3 cells were used since they overexpress the membrane receptor erbB2 that can be specifically targeted by the antibody on the particles. The SK-BR-3 cells were incubated on glass coverslips with **PR-AuNP-PEG-Ab** conjugates (0.8 µM porphyrin equivalent) for 3 h.

Following incubation, the coverslips containing the SK-BR-3 cells were washed to remove any excess **PR-AuNP-PEG-Ab** and placed in a Ludin chamber at 37 °C in a fluorescence microscope. Since the porphyrin based ligands are fluorescent, it is possible to visualise the uptake of the **PR-AuNP-PEG-Ab** conjugates by the cells using fluorescence microscopy. **Figure 6** shows images of the SK-BR-3 cells that had been incubated with the **PR-AuNP-PEG-Ab** conjugates. Control cells with no nanoparticles loaded were also imaged and are shown in **Figure 6**. These images, in particular the comparison between **Figure 6** (**b** and **e**), clearly demonstrate the high level of cellular uptake of the **PR-AuNP-PEG-Ab** conjugates by the breast cancer cell line. The intense red fluorescence emission observed inside the cells treated with **PR-AuNP-PEG-Ab** conjugates (**Figure 6b**) was not observed in the control cells (**Figure 6e**).

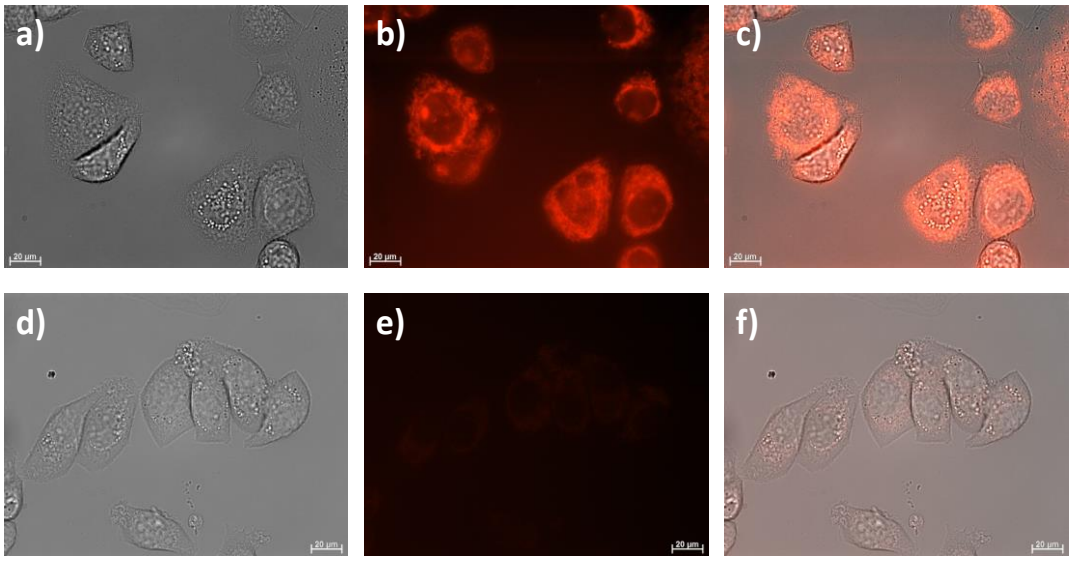


**Figure 6**. Bright field and fluorescence images of SK-BR-3 cells before irradiation to produce singlet oxygen: **a – c)** cells loaded with **PR-AuNP-PEG-Ab** conjugates and **d – f)** control cells without nanoparticles loaded. Images correspond to: bright field images (**a** and **d**); fluorescence images due to the fluorescence of the porphyrin on the nanoparticles (**b** and **e**) and composite images of bright field and fluorescence (**c** and **f**). Scale bars = 20 µm.

To activate the generation of singlet oxygen, SK-BR-3 cells loaded with the **PR-AuNP-PEG-Ab** conjugates were irradiated with the light from a mercury arc lamp for 30 s. Following irradiation of the cells, propidium iodide was added to stain the dead cells.[32] When cells loaded with the **PR-AuNP-PEG-Ab** conjugates were irradiated to induce singlet oxygen production, morphological changes were observed (**Figure 7 a-c**). The cell membranes of these treated cells appear damaged as confirmed by the propidium iodide staining of their nucleus (**Figure 7b**). Propidium iodide cannot bind to the nucleic acids of non-damaged cells since it is excluded by healthy cell membranes. The irradiated control cells, without nanoparticles loaded, show no staining with the propidium iodide (**Figure 7d-f**), indicating that the cells were viable.

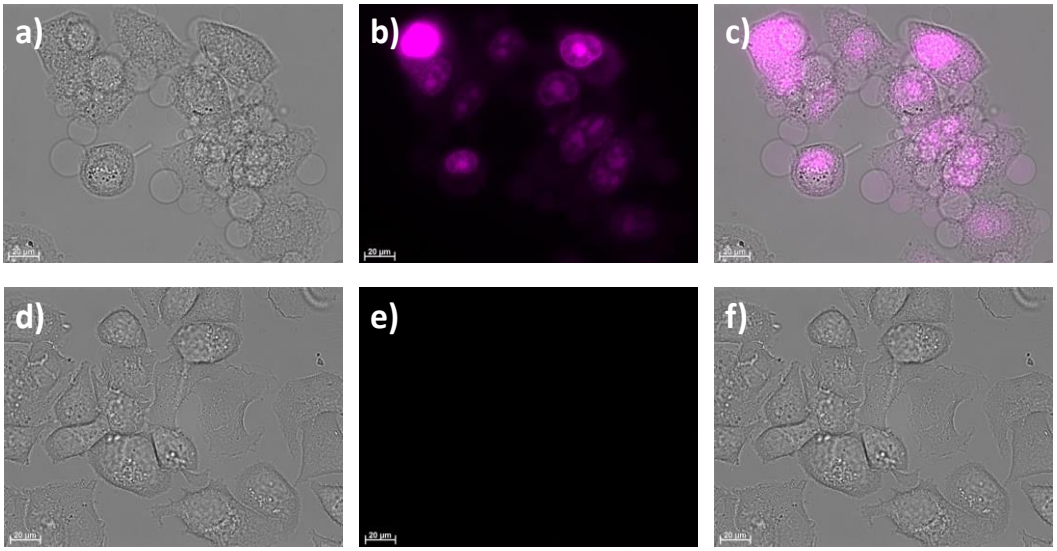


**Figure 7**. Bright field and fluorescence images of SK-BR-3 cells 8 min after irradiation, to produce singlet oxygen, and loaded with propidium iodide to stain dead cells: **a – c)** cells loaded with **PR-AuNP-PEG-Ab** conjugates and **d – f)** control cells without nanoparticles loaded. Images correspond to: bright field images (**a** and **d**); fluorescence images due to the fluorescence of the propidium iodide (**b** and **e**) and composite images of bright field and fluorescence (**c** and **f**). Only the SK-BR-3 cells following PDT with the **PR-AuNP-PEG-Ab** conjugates stained positive for propidium iodide (**a** – **c**). Scale bars = 20 µm.

## CONCLUSIONS

Treatment of cancer can be achieved in a targeting manner using ligands such as antibodies that are able to specifically recognise and bind to cell surface receptors expressed only on the cancer cell. Nanoparticles have recently emerged as ideal delivery vehicles in the treatment of cancer by PDT since they allow for the aqueous based delivery of hydrophobic photosensitizers and can be further used as platforms for the conjugation of targeting agents. Thus, nanoparticle conjugates can be used to selectively recognise tumour tissues and to treat them *via* photodynamic therapy.[5,33] To the best of our knowledge, the synthesis and application of a water soluble gold nanoparticle-based conjugate that combines the functionalisation of gold nanoparticles with a porphyrin photosensitizer derivative, together with a PEG derivative ligand and an antibody for the targeted PDT of cancer cells has not been previously reported. In the work presented herein, a porphyrin derivative, **PR-SH**, together with a PEG derivative have been used to synthesise water soluble gold nanoparticles. When designing a conjugate to be used for PDT applications, a high production of singlet oxygen following irradiation of the photosensitizer is required. To date, different protocols have been reported for the synthesis of water soluble gold nanoparticles containing hydrophobic ligands including hydrophobic photosensitizers. In the research here presented, the gold nanoparticle conjugates were synthesised following two different protocols with the aim of determining the optimum method for targeted PDT applications. The first synthetic method was based on a biphasic method in which water and toluene were used as solvents and TOAB is used to enable the phase transfer of the reagents.[10] This synthetic method yielded **PR-AuNP-PEG** (biphasic) of *ca.* 4.5 nm in diameter. The second synthetic method used a combination of DMF and THF as solvents which are miscible and therefore allowed the synthesis of the nanoparticles in a monophasic environment.[22]

The **PR-AuNP-PEG** (monophasic) were *ca.* 9 nm in diameter. Non-water soluble nanoparticles (**PR-AuNP**) containing the ligand **PR-SH** were also synthesised following the biphasic method for comparison. The free ligand and the synthesised nanoparticles were characterised using different spectroscopic techniques, UV-Vis absorption and fluorescence spectroscopies, together with transmission electron microscopy and zeta potential measurements. The results obtained from the spectroscopic characterisation confirmed the functionalisation of the nanoparticles with the porphyrin derivative ligand and, in combination with TEM results, allowed for an estimation of the porphyrin ligand per nanoparticle on each type of nanoparticles (56, 3882 and 678 **PR-SH**/AuNP for **PR-AuNP-PEG** (biphasic), **PR-AuNP-PEG** (monophasic) and **PR-AuNP**, respectively). These results determined that those water soluble **PR-AuNP-PEG** nanoparticles synthesised using the monophasic method contained more porphyrin derivative ligands per nanoparticle than the nanoparticles synthesised following the biphasic method. The ability of the nanoparticles to produce singlet oxygen was investigated by measuring the maximum ratio of ADPA photobleaching following irradiation with blue light. The production of singlet oxygen by the porphyrin derivative ligand was enhanced when the ligand was attached to the surface of gold nanoparticles. The water insoluble particles containing only **PR-SH**, produced the highest level of singlet oxygen, since the production was measured in DCM where the lifetime of singlet oxygen is considerably longer than in comparison to aqueous media. Amongst the water soluble nanoparticles, the **PR-AuNP-PEG** (monophasic) produced higher levels of singlet oxygen than the **PR-AuNP-PEG** (biphasic), making those nanoparticle conjugates the optimal candidates for use in PDT. **PR-AuNP-PEG** (monophasic) were further covalently functionalised with the antibody anti-erbB2 to target the erbB2 receptors expressed on the surface of breast cancer SK-

BR-3 cells with the aim of achieving targeted PDT. The **PR-AuNP-PEG-Ab** yielded a slightly lower % rate of ADPA photobleaching than the **PR-AuNP-PEG** (monophasic) in aqueous solution but had the advantage of containing a targeting agent for tumor selectivity. The **PR-AuNP-PEG-Ab** conjugates were used to induce the death of SK-BR-3 breast cancer cells *via* PDT. The cells were incubated with the **PR-AuNP-PEG-Ab** conjugates demonstrating a high level of cellular uptake. Following irradiation of the SK-BR-3 cancer cells incubated with the **PR-AuNP-PEG-Ab** conjugates, changes in the cellular morphology were observed and cell membrane damage was confirmed using staining with propidium iodide. The water soluble anti-erbB2 antibody-porphyrin conjugates reported in this work were shown to selectively target the erbB2 receptor that is overexpressed on SK-BR-3 breast cancer cells and are thus, ideal conjugates for the targeted PDT treatment of breast cancer cells. These results demonstrate that gold nanoparticle conjugates containing porphyrin derivatives as photosensitizers and antibodies as targeting agents covalently attached to PEG that provides water solubility may have a great potential for PDT of cancer. The research here reported will be extended further with the use of the nanoparticle-conjugates for *in vivo* treatment of breast cancer following PDT. Furthermore, by using different antibodies, similar 4-component conjugates will be designed for targeting and treatment of various types of cancers.

## ACKNOWLEDGEMENTS

This work was supported by the EU ERDF (FEDER) funds and the Spanish Government grant TEC2014-51940-C2-2-R. O.P. thanks the MINECO for a predoctoral grant. M.J.M. was funded by the School of Chemistry, University of East Anglia.

## SUPPLEMENTARY MATERIAL

Supplementary material for this article is available in the online version. (1) Schematic representation of the **PR-AuNP-PEG** nanoparticle conjugates: gold nanoparticles functionalised with the thiolated porphyrin derivative ligand (red) and the thiolated polyethylene glycol derivative ligand (black) (Figure S1); (2) Schematic representation of the **PR-AuNP** conjugates: gold nanoparticles functionalised with the thiolated porphyrin derivative ligand (Figure S2); (3) **a)** Transmission electron micrograph and **b)** corresponding size distribution histogram of **PR-AuNP** (Figure S3); (4) **a)** UV-Vis absorption spectra of **PR-SH** at varying concentrations (from 0.5 to 15 μM) and **b)** resulting calibration curve plotting the absorbance at $\lambda$ = 418 nm (Soret band) as a function of the concentration of **PR-SH** (Figure S4); (5) UV-Visible extinction spectra used to calculate the contribution of **PR-SH** to the extinction intensity of: **a) PR-AuNP-PEG** (biphasic), **b) PR-AuNP-PEG** (monophasic) and **c) PR-AuNP**. To calculate the contribution of the ligands to the total extinction intensity (red lines), extinction intensity at $\lambda$ = 460 nm due to the AuNPs has to be subtracted from the total extinction intensity maximum for **PR-AuNP-PEG** and **PR-AuNP** (Figure S5); (6) Calculations for the concentration of **PR-SH** on the different functionalised nanoparticles: **PR-AuNP-PEG** synthesised following the biphasic and the monophasic methods and **PR-AuNP** (Figure S6); (7) Fluorescence excitation spectra of **PR-SH** (0.25 mM – black); **PR-AuNP** (blue); and **PR-AuNP-PEG** synthesised following the biphasic method (0.4 mg/mL in water – green) and the monophasic method (0.4 mg/mL in water – red). The spectra of **PR-SH** and **PR-AuNP** were recorded using em/ex slits = 5 while the spectra of **PR-AuNP-PEG** were recorded using em/ex slits = 10. Inset: magnification of the fluorescence excitation spectra in the region between $\lambda$ = 490 – 675 nm (Figure S7); (8) UV-Vis extinction spectrum of **PR-AuNP-PEG-Ab** in water (Figure S8); (9) Zeta

potential values of **PR-AuNP-PEG** and **PR-AuNP-PEG-Ab**. All of the measurements were performed in triplicate. The particles were dispersed in PBS (pH 7.4) (Table S1); (10) Time-dependent decay of ADPA absorption spectrum as a result of the photobleaching of the singlet oxygen probe upon irradiation of: **a) PR-SH**, **b) PR-AuNP**, **c) PR-AuNP-PEG** (biphasic), **d) PR-AuNP-PEG** (monophasic) and **e) PR-AuNP-PEG-Ab** in the presence of ADPA in DCM for **PR-SH** and **PR-AuNP** and in aqueous solution for **PR-AuNP-PEG** and **PR-AuNP-PEG-Ab**. The samples were irradiated for 4 h (3 h for **PR-AuNP-PEG** (biphasic)) with a blue light source ($\lambda$ = 400 – 500 nm) (Figure S9); (11) Percentage decay of ADPA photobleaching at $\lambda$ = 378 nm following irradiation (400 – 500 nm) of: **PR-SH** (black line) **PR-AuNP** (red line), **PR-AuNP-PEG** (biphasic) (green line), **PR-AuNP-PEG** (monophasic) (blue line) and **PR-AuNP-PEG-Ab** (cyan line). The percentage decay of ADPA photobleaching for **PR-SH** and **PR-AuNP** was performed in DCM while for **PR-AuNP-PEG** and **PR-AuNP-PEG-Ab** the photobleaching was measured in an aqueous solution (Figure S10).

## REFERENCES


(1) Dougherty, T. J., Gomer, C. J., Henderson, B. W., Jori, G., Kessel, D., Korbelik, M., Moan, J., and Peng, Q. (1998) Photodynamic therapy. *J. Natl. Cancer Inst. 90*, 889-905.

(2) DeRosa, M. C., and Crutchley, R. J. (2002) Photosensitized singlet oxygen and its applications. *Coord. Chem. Rev. 233–234*, 351-371.

(3) Ormond, A. B., and Freeman, H. S. (2013) Dye sensitizers for photodynamic therapy. *Materials 6*, 817-840.

(4) ori, G. (1996) Tumour photosensitizers: approaches to enhance the selectivity and efficiency of photodynamic therapy. *J. Photochem. Photobiol., B 36*, 87-93.

(5) Obaid, G., and Russell, D. A. (2013) Nanoparticles for photodynamic cancer therapy. *Handbook of photomedicine* (Hamblin, M. R., and Huang, Y.-Y., Eds.) pp 367-378, Taylor & Francis, CRC Press: Boca Raton, FL.

(6) Couleaud, P., Morosini, V., Frochot, C., Richeter, S., Raehm, L., and Durand, J.-O. (2010) Silica-based nanoparticles for photodynamic therapy applications. *Nanoscale 2*, 1083-1095.

(7) Bechet, D., Couleaud, P., Frochot, C., Viriot, M. L., Guillemin, F., and Barberi-Heyob, M. (2008) Nanoparticles as vehicles for delivery of photodynamic therapy agents. *Trends Biotechnol. 26*, 612-621.

(8) Juzenas, P., Chen, W., Sun, Y.-P., Coelho, M. A. N., Generalov, R., Generalova, N., and Christensen, I. L. (2008) Quantum dots and nanoparticles for photodynamic and radiation therapies of cancer. *Adv. Drug Delivery Rev. 60*, 1600-1614.

(9) Wang, C., Cheng, L., and Liu, Z. (2013) Upconversion nanoparticles for photodynamic therapy and other cancer therapeutics. *Theranostics 3*, 317-330.

(10) Brust, M., Walker, M., Bethell, D., Schiffrin, D. J., and Whyman, R. (1994) Synthesis of thiol-derivatised gold nanoparticles in a two-phase liquid-liquid system. *J. Chem. Soc., Chem. Commun.* 801-802.

(11) Hone, D. C., Walker, P. I., Evans-Gowing, R., FitzGerald, S., Beeby, A., Chambrier, I., Cook, M. J., and Russell, D. A. (2002) Generation of cytotoxic singlet oxygen *via* phthalocyanine-stabilized gold nanoparticles: a potential delivery vehicle for photodynamic therapy. *Langmuir 18*, 2985-2987.

(12) Wieder, M. E., Hone, D. C., Cook, M. J., Handsley, M. M., Gavrilovic, J., and Russell, D. A. (2006) Intracellular photodynamic therapy with photosensitizer-nanoparticle conjugates: cancer therapy using a 'Trojan horse'. *Photochem. Photobiol. Sci. 5*, 727-734.

(13) Gamaleia, N. F., Shishko, E. D., Dolinsky, G. A., Shcherbakov, A. B., Usatenko, A. V., and Kholin, V. V. (2010) Photodynamic activity of hematoporphyrin conjugates with gold nanoparticles: experiments *in vitro*. *Exp. Oncol. 32*, 44-47.

(14) Khaing Oo, M. K., Yang, Y., Hu, Y., Gomez, M., Du, H., and Wang, H. (2012) Gold nanoparticle-enhanced and size-dependent generation of reactive oxygen species from protoporphyrin IX. *ACS Nano 6*, 1939-1947.

(15) Zaruba, K., Kralova, J., Rezanka, P., Pouckova, P., Veverkova, L., and Kral, V. (2010) Modified porphyrin-brucine conjugated to gold nanoparticles and their application in photodynamic therapy. *Org. Biomol. Chem. 8*, 3202-3206.

(16) Cheng, Y., A, C. S., Meyers, J. D., Panagopoulos, I., Fei, B., and Burda, C. (2008) Highly efficient drug delivery with gold nanoparticle vectors for *in vivo* photodynamic therapy of cancer. *J. Am. Chem. Soc. 130*, 10643-10647.

(17) Cheng, Y., Meyers, J. D., Agnes, R. S., Doane, T. L., Kenney, M. E., Broome, A.-M., Burda, C., and Basilion, J. P. (2011) Addressing brain tumors with targeted gold nanoparticles: a new gold standard for hydrophobic drug delivery? *Small 7*, 2301-2306.

(18) Cheng, Y., Meyers, J. D., Broome, A.-M., Kenney, M. E., Basilion, J. P., and Burda, C. (2011) Deep penetration of a PDT drug into tumors by noncovalent drug-gold nanoparticle conjugates. *J. Am. Chem. Soc. 133*, 2583-2591.

(19) Meyers, J. D., Cheng, Y., Broome, A.-M., Agnes, R. S., Schluchter, M. D., Margevicius, S., Wang, X., Kenney, M. E., Burda, C., and Basilion, J. P. (2015) Peptide-targeted gold nanoparticles for photodynamic therapy of brain cancer. *Part. Part. Syst. Charact. 32*, 448-457.

(20) Camerin, M., Moreno, M., Marín, M. J., Schofield, C. L., Chambrier, I., Cook, M. J., Coppellotti, O., Jori, G., and Russell, D. A. (2016) Delivery of a hydrophobic

phthalocyanine photosensitizer using PEGylated gold nanoparticle vonjugates for the *in vivo* photodynamic therapy of amelanotic melanoma. *Photochem. Photobiol. Sci. 15*, 618-625.

(21) Stuchinskaya, T., Moreno, M., Cook, M. J., Edwards, D. R., and Russell, D. A. (2011) Targeted photodynamic therapy of breast cancer cells using antibody-phthalocyanine-gold nanoparticle conjugates. *Photochem. Photobiol. Sci. 10*, 822-831.

(22) Obaid, G., Chambrier, I., Cook, M. J., and Russell, D. A. (2012) Targeting the oncofetal Thomsen–Friedenreich disaccharide using jacalin-PEG phthalocyanine gold nanoparticles for photodynamic cancer therapy. *Angew. Chem., Int. Ed. 51*, 6158-6162.

(23) Obaid, G., Chambrier, I., Cook, M. J., and Russell, D. A. (2015) Cancer targeting with biomolecules: a comparative study of photodynamic therapy efficacy using antibody or lectin conjugated phthalocyanine-PEG gold nanoparticles. *Photochem. Photobiol. Sci. 14*, 737-747.

(24) Penon, O., Marín, M. J., Amabilino, D. B., Russell, D. A., and Pérez-García, L. (2016) Iron oxide nanoparticles functionalized with novel hydrophobic and hydrophilic porphyrins as potential agents for photodynamic therapy. *J. Colloid Interface Sci. 462*, 154-165.

(25) Penon, O., Patiño, T., Barrios, L., Nogués, C., Amabilino , D. B., Wurst, K., and Pérez-García, L. A (2015) New porphyrin for the preparation of functionalized water-soluble gold nanoparticles with low intrinsic toxicity. *ChemistryOpen 4*, 127-136.

(26) Lindig, B. A., Rodgers, M. A. J., and Schaap, A. P. (1980) Determination of the lifetime of singlet oxygen in $D_2O$ using 9,10-anthracenedipropionic acid, a water-soluble probe. *J. Am. Chem. Soc. 102*, 5590-5593.

(27) Zheng, W., Shan, N., Yu, L., and Wang, X. (2008) UV–visible, fluorescence and EPR properties of porphyrins and metalloporphyrins. *Dyes Pigm. 77*, 153-157.

(28) Haiss, W., Thanh, N. T., Aveyard, J., and Fernig, D. G. (2007) Determination of size and concentration of gold nanoparticles from UV-vis spectra. *Anal. Chem. 79*, 4215-4221.

(29) Mano, M. (2006) Vinorelbine in the management of breast cancer: new perspectives, revived role in the era of targeted therapy. *Cancer Treat. Rev. 32*, 106-118.

(30) Whitaker, J. R., and Granum, P. E. (1980) An absolute method for protein determination based on difference in absorbance at 235 and 280 nm. *Anal. Biochem. 109*, 156-159.

(31) Durmus, M. (2012) *Photosensitizers in Medicine, Environment, and Security* (Nyokong, T., and Ahsen, V., Eds.) pp 149-151, Springer Science & Business Media, Dordrecht.

(32) Riccardi, C., and Nicoletti, I. (2006) Analysis of apoptosis by propidium iodide staining and flow cytometry. *Nat. Protocols 1*, 1458-1461.

(33) Calavia, P. G.; Russell, D. A.: CHAPTER 7 Metallic Nanoparticles for Targeted Delivery of Photosensitisers for Photodynamic Therapy. In *Photodynamic Medicine: From Bench to Clinic*; The Royal Society of Chemistry, 2016; pp 113-135.

# SUPPLEMENTARY MATERIAL

# Water soluble, multifunctional antibody-porphyrin gold nanoparticles for targeted photodynamic therapy

Oriol Penon,[†] María J. Marín,[*,‡] David A. Russell,[‡] Lluïsa Pérez-García,[*,†,§]

[†] Departament de Farmacologia, Toxicologia i Química Terapèutica and Institut de Nanociència i Nanotecnología UB (IN2UB), Universitat de Barcelona, Avda. Joan XXIII 27-31, 08028 Barcelona, Spain.

[‡] School of Chemistry, University of East Anglia, Norwich Research Park, Norwich, Norfolk, NR4 7TJ, UK.

[§] Present address: School of Pharmacy, The University of Nottingham, University Park, Nottingham NG72RD, England, UK.

LIST OF CONTENTS

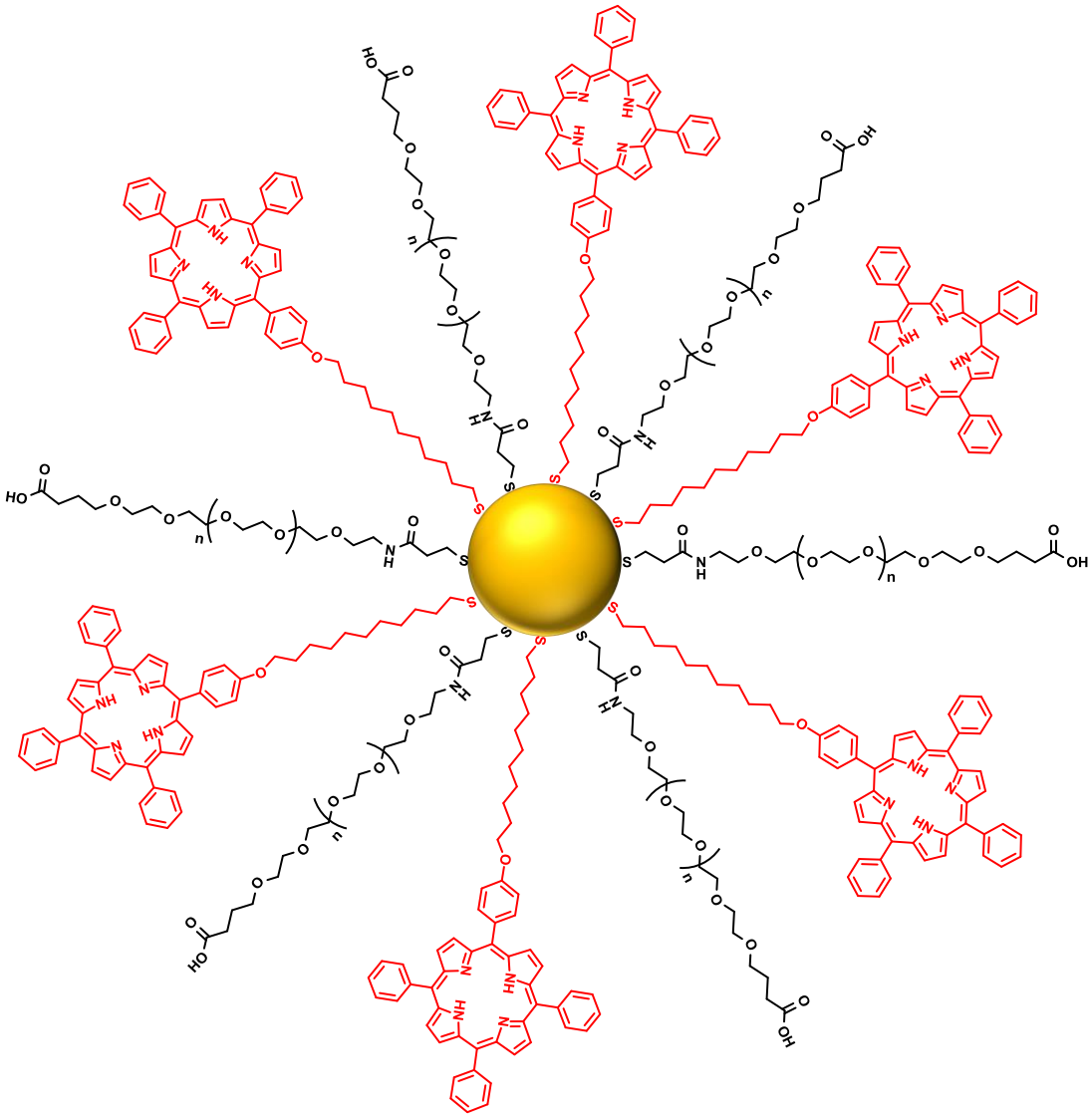

**Figure S1**. Schematic representation of the **PR-AuNP-PEG** nanoparticle conjugates: gold nanoparticles functionalised with the thiolated porphyrin derivative ligand (red) and the thiolated polyethylene glycol derivative ligand (black).

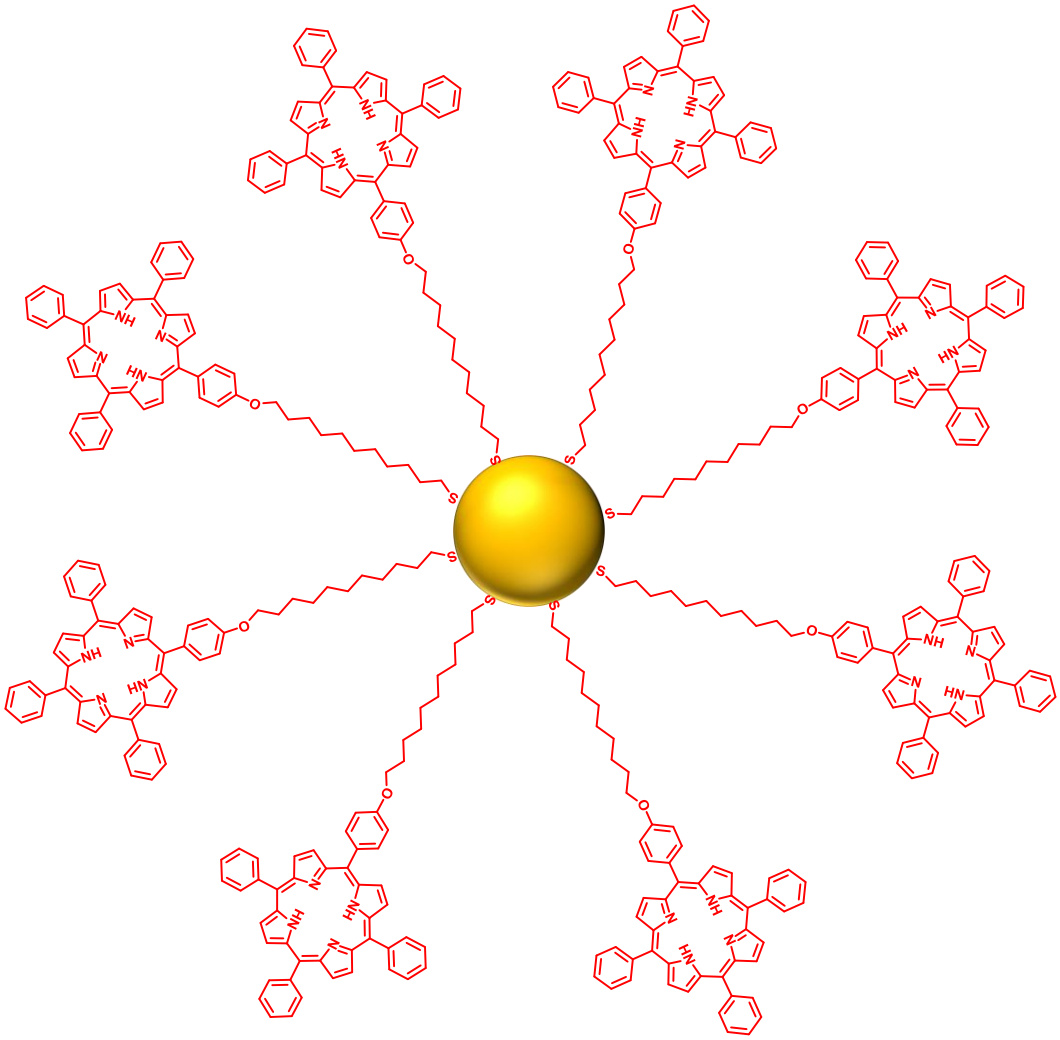

**Figure S2**. Schematic representation of the **PR-AuNP** conjugates: gold nanoparticles functionalised with the thiolated porphyrin derivative ligand.

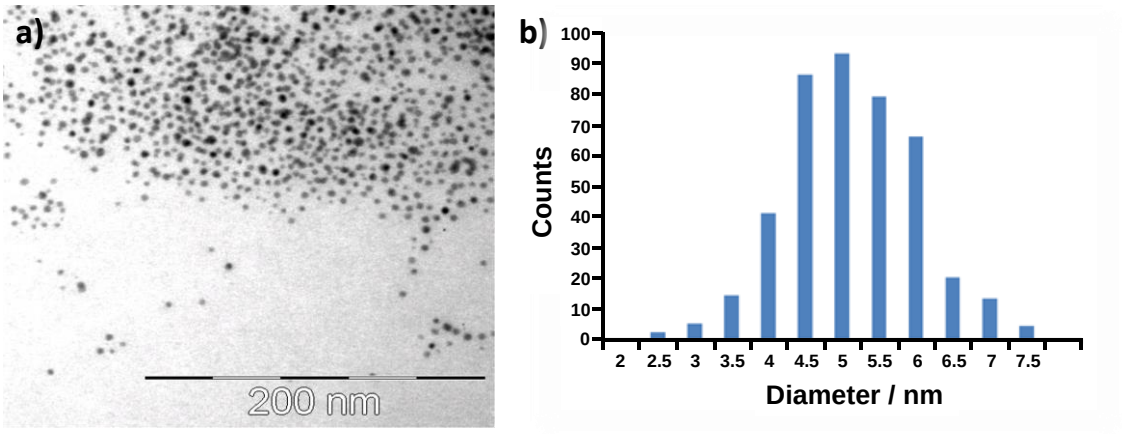


**Figure S3**. **a)** Transmission electron micrograph and **b)** corresponding size distribution histogram of **PR-AuNP**.

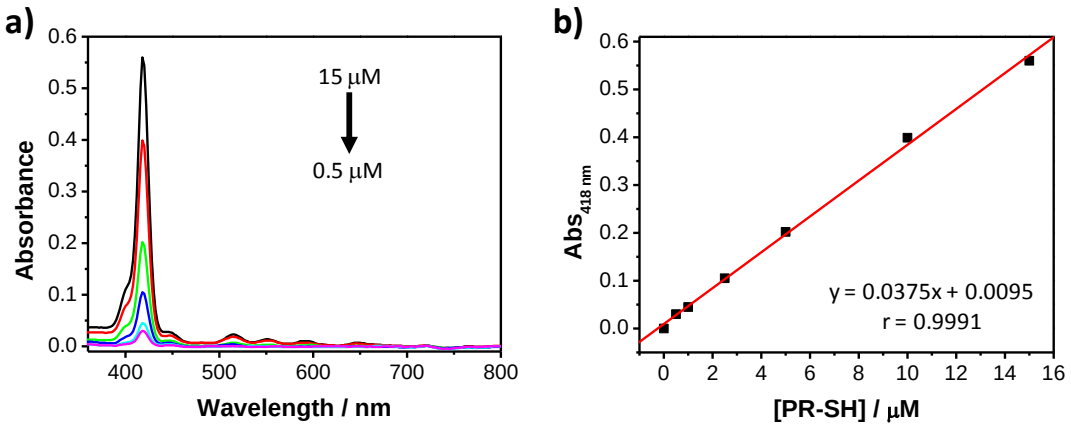


**Figure S4**. **a)** UV-Vis absorption spectra of **PR-SH** at varying concentrations (from 0.5 to 15 µM) and **b)** resulting calibration curve plotting the absorbance at λ = 418 nm (Soret band) as a function of the concentration of **PR-SH**.

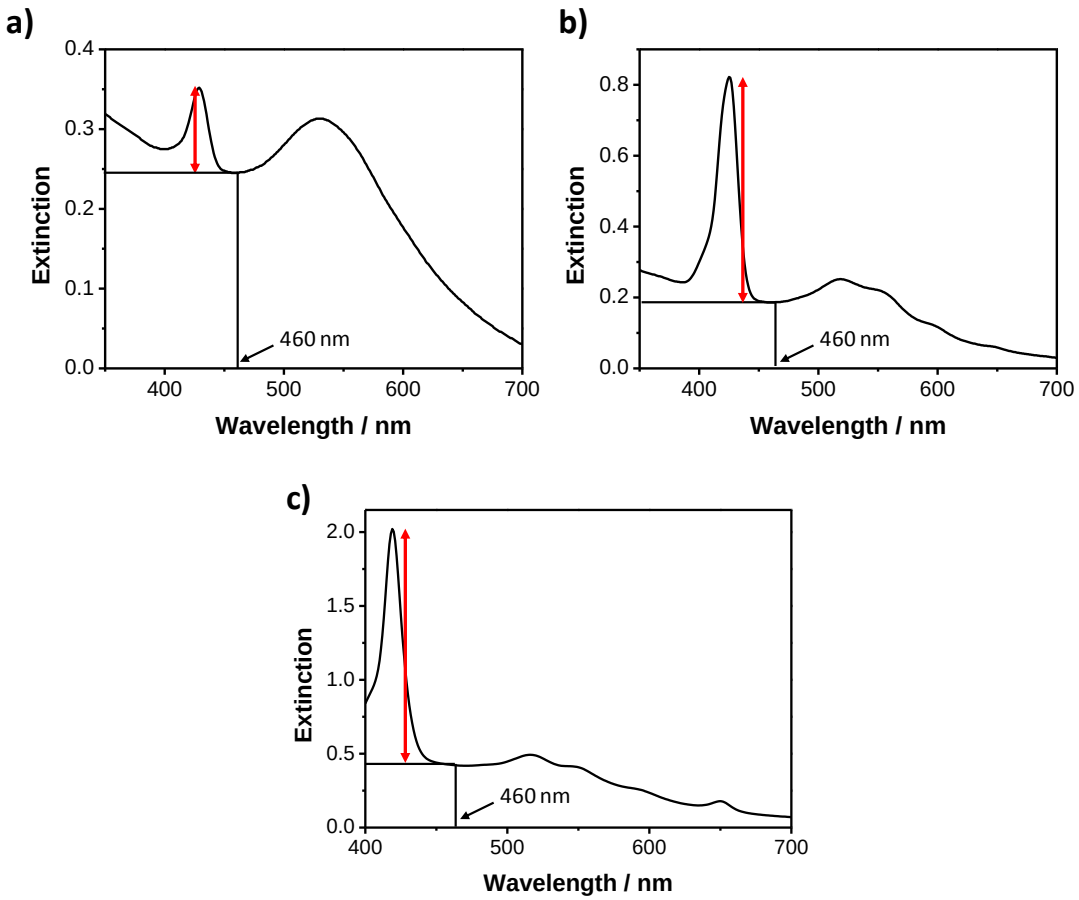


**Figure S5**. UV-Visible extinction spectra used to calculate the contribution of **PR-SH** to the extinction intensity of: **a) PR-AuNP-PEG** (biphasic), **b) PR-AuNP-PEG** (monophasic) and **c) PR-AuNP**. To calculate the contribution of the ligands to the total extinction intensity (red lines), extinction intensity at $\lambda$ = 460 nm due to the AuNPs has to be subtracted from the total extinction intensity maximum for **PR-AuNP-PEG** and **PR-AuNP**.

**PR-AuNP-PEG (biphasic)**

**PR-SH** concentration on AuNPs:

- $Abs = Abs_{430nm} - Abs_{460nm}$

$Abs = 0.350 - 0.245 = 0.105$

Applying the calibration curved obtained in Figure S4:

$$Abs = 0.0375 \times C_{PR\text{-}SH\ -\ \mu M} + 0.0095$$

$$C_{PR\text{-}SH} = \frac{Abs - 0.0095}{0.0375}$$

$C_{PR\text{-}SH} = 2.55\ \mu M$

**PR-AuNP-PEG (monophasic)**

**PR-SH** concentration on AuNPs:

- $Abs = Abs_{426nm} - Abs_{460nm}$

$Abs = 0.820 - 0.186 = 0.634$

Applying the calibration curved obtained in Figure S4:

$$Abs = 0.0375 \times C_{PR\text{-}SH\ -\ \mu M} + 0.0095$$

$$C_{PR\text{-}SH} = \frac{Abs - 0.0095}{0.0375}$$

$C_{PR\text{-}SH} = 16.65\ \mu M$

**PR-AuNP**

**PR-SH** concentration on AuNPs:

- $Abs = Abs_{418nm} - Abs_{460nm}$

$Abs = 1.990 - 0.425 = 1.563$

Applying the calibration curved obtained in Figure S4:

$$Abs = 0.0375 \times C_{PR\text{-}SH\ -\ \mu M} + 0.0095$$

$$C_{PR\text{-}SH} = \frac{Abs - 0.0095}{0.0375}$$

$C_{PR\text{-}SH} = 41.43\ \mu M$

**Figure S6**. Calculations for the concentration of **PR-SH** on the different functionalised nanoparticles: **PR-AuNP-PEG** synthesised following the biphasic and the monophasic methods and **PR-AuNP**.

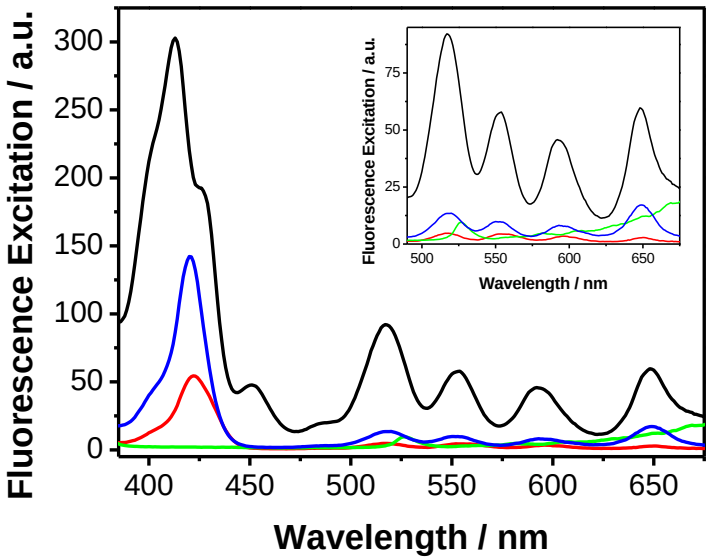


**Figure S7**. Fluorescence excitation spectra of **PR-SH** (0.25 mM – black); **PR-AuNP** (blue); and **PR-AuNP-PEG** synthesised following the biphasic method (0.4 mg/mL in water – green) and the monophasic method (0.4 mg/mL in water – red). The spectra of **PR-SH** and **PR-AuNP** were recorded using em/ex slits = 5 while the spectra of **PR-AuNP-PEG** were recorded using em/ex slits = 10. Inset: magnification of the fluorescence excitation spectra in the region between $\lambda$ = 490 – 675 nm.

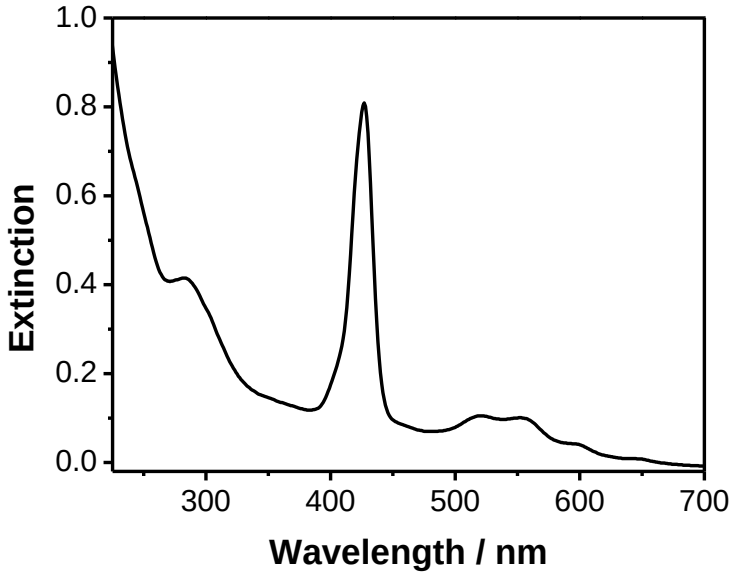


**Figure S8**. UV-Vis extinction spectrum of **PR-AuNP-PEG-Ab** in water.

**Table S1.** Zeta potential values of **PR-AuNP-PEG** and **PR-AuNP-PEG-Ab**. All of the measurements were performed in triplicate. The particles were dispersed in PBS (pH 7.4).

| Sample | Zeta potential (mV) |
|---|---|
| **PR-AuNP-PEG (biphasic)** | -21.96 ± 1.0 |
| **PR-AuNP-PEG (monophasic)** | -11.76 ± 0.3 |
| **PR-AuNP-PEG-Ab** | 0.04 ± 0.1 |

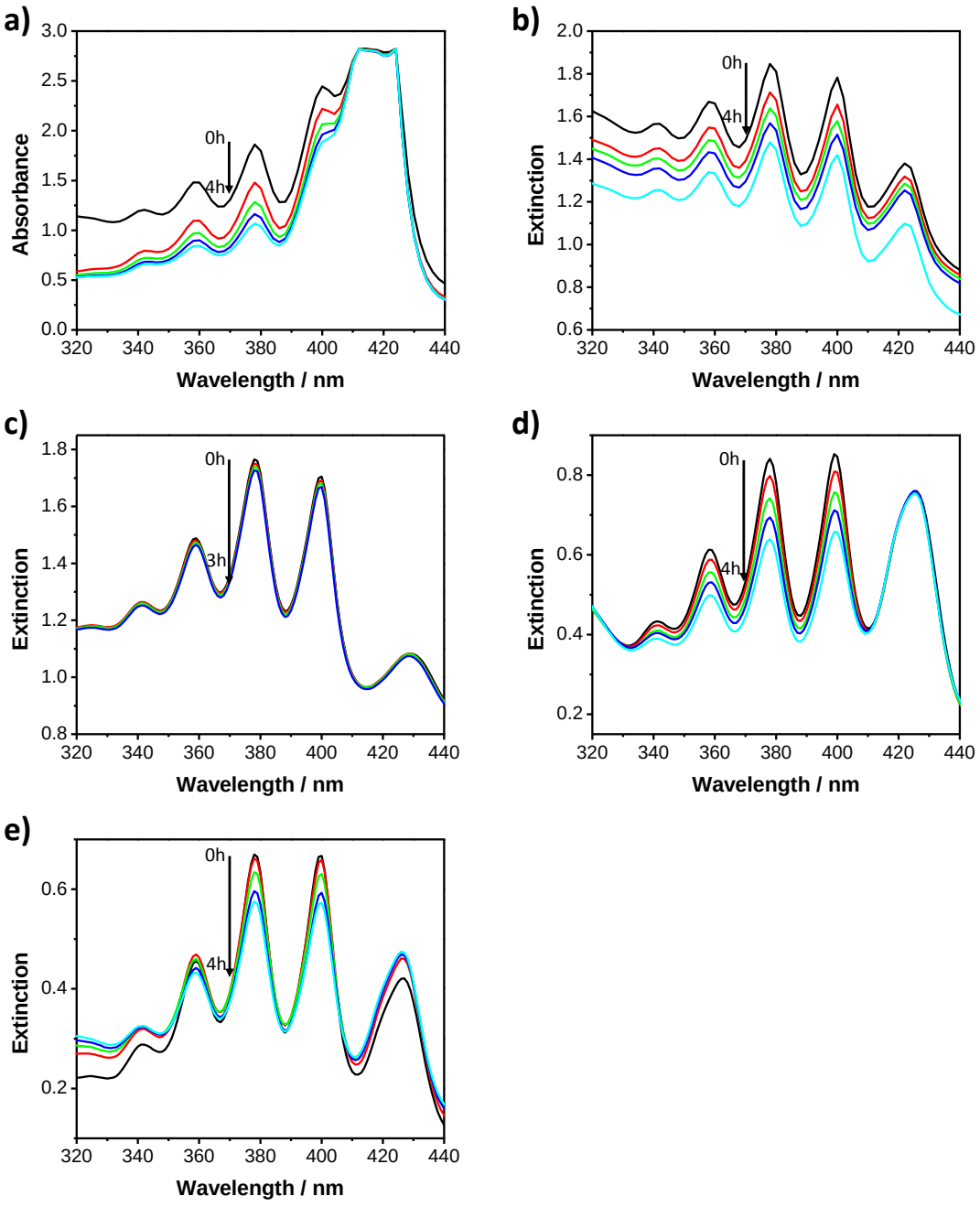


**Figure S9**. Time-dependent decay of ADPA absorption spectrum as a result of the photobleaching of the singlet oxygen probe upon irradiation of: **a) PR-SH**, **b) PR-AuNP**, **c) PR-AuNP-PEG** (biphasic), **d) PR-AuNP-PEG** (monophasic) and **e) PR-AuNP-PEG-Ab**, in the presence of ADPA in DCM for **PR-SH** and **PR-AuNP**, and in aqueous solution for **PR-AuNP-PEG** and **PR-AuNP-PEG-Ab**. The samples were irradiated for 4 h (3 h for **PR-AuNP-PEG** (biphasic)) with a blue light source ($\lambda$ = 400 – 500 nm).

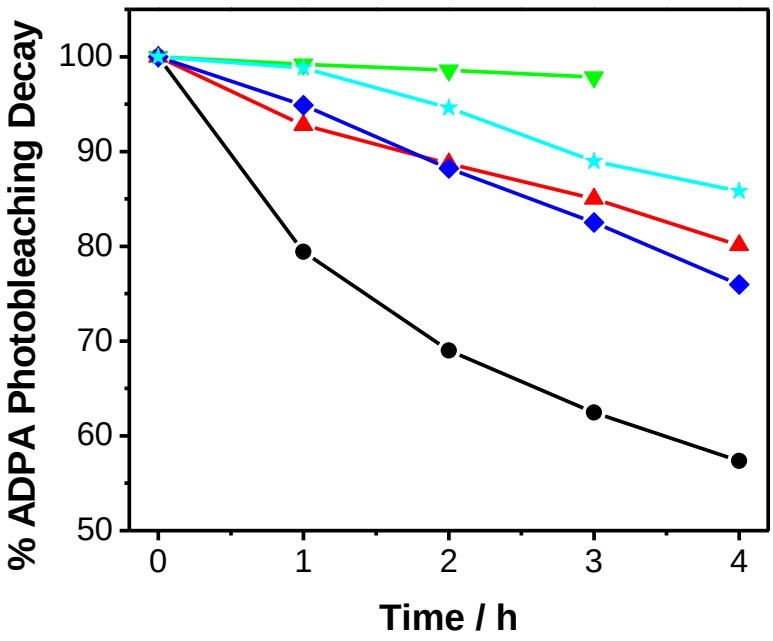


**Figure S10**. Percentage decay of ADPA photobleaching at λ = 378 nm following irradiation (400 – 500 nm) of: **PR-SH** (black line) **PR-AuNP** (red line), **PR-AuNP-PEG** (biphasic) (green line), **PR-AuNP-PEG** (monophasic) (blue line) and **PR-AuNP-PEG-Ab** (cyan line). The percentage decay of ADPA photobleaching for **PR-SH** and **PR-AuNP** was performed in DCM while for **PR-AuNP-PEG** and **PR-AuNP-PEG-Ab** the photobleaching was measured in an aqueous solution.